

Surface effects on nonlinear vibration and buckling analysis of embedded FG nanoplates via refined HOSDPT in hygrothermal environment considering physical neutral surface position

Farzad Ebrahimi* and Ebrahim Heidari

*Department of Mechanical Engineering, Faculty of Engineering, Imam Khomeini International University,
Qazvin*

(Received May 5, 2018, Revised June 6, 2018, Accepted June 15, 2018)

Abstract. In this paper the hygro-thermo-mechanical vibration and buckling behavior of embedded FG nanoplates are investigated. The Eringen's and Gurtin-Murdoch theories are applied to study the small scale and surface effects on frequencies and critical buckling loads. The effective material properties are modeled using Mori-Tanaka homogenization scheme. On the base of RPT and HSDPT plate theories, the Hamilton's principle is employed to derive governing equations. Using iterative and GDQ methods the governing equations are solved and the influence of different parameters on natural frequencies and critical buckling loads are studied.

Keywords: nanomechanics; rectangular plate; hygro-thermo-mechanical; surface effect; generalized differential quadrature method; high shear deformation plate theory; thermal loading; elastic medium; nonlocal; neutral axis

1. Introduction

Nano-material have recently attracted a lot of attention Because of superior mechanical, thermal and electrical properties; considering these properties, different field of studies have been developed; for example, some studies focus on mechanical properties (Bellifa, Benrahou, and Bousahala 2017, Karami, Janghorban and Tounsi 2018a, Bouafia *et al.* 2017, Youcef *et al.* 2018, Ahouel *et al.* 2016, Mokhtar *et al.* 2018, Karami, Janghorban and Tounsi 2018b, Chaht *et al.* 2015); in addition to mechanical properties some studies consider thermal properties (Khetir *et al.* 2017, Ebrahimi and Barati 2016a, b, 2018a, Ebrahimi and Salari 2015); electrical and mechanical properties are another subject that has attracted the attention of researchers (Shen, Wang and Zheng 2018, Ebrahimi and Barati 2016c, d, 2017c, 2018b). There are specified methods for modeling these structures and driving related equations which are solved by analytical or numerical methods (Akgöz and Civalek 2016, 2011, Civalek and Demir 2016, Chen and Li 2013, Mercan and Civalek 2016, Gürses *et al.* 2009, Civalek 2013, Ebrahimi and Shafiei 2017). Nano-plates, as one of the nano-structures, are used a lot in nano/micro-electromechanical systems

*Corresponding author, Professor, E-mail: febrahimi@eng.ikiu.ac.ir

(NEMS/MEMS) (Gholami, Ansari and Gholami 2017) and there are many researches which study nano-plates for situations that are applicable for these systems (Yazid *et al.* 2018, Bounouara *et al.* 2016, Besseghier *et al.* 2017, Ebrahimi, Hamed and Hosseini 2016, 2017d, Ebrahimi and Hosseini 2016b). The buckling behavior of nano-plates with nonlocal elasticity and surface stress theories have been studied by Karimi and Shahidi (2015) using finite difference method. Foroushani and Azhari (2016) investigated the buckling and vibration behavior of thick rectangular nano-plates based on Reddy's plate theory; using finite strip method they concluded that for thick plates, the critical buckling load and natural frequency are intensely dependent on the nonlocal parameter, whereas the effect of the effect of geometrical parameters are more important when the plate is thin. Ebrahimi and Barati (2017a) studied damping vibration of smart piezoelectric nano-plates using strain gradient theory. Based on classical plate theory and first order shear deformation theory Habibi *et al.* (2016) investigated the characteristic of the vibration of the nano-plate which is placed on elastic foundation in thermal environment. Ansari and Gholami (2017) used Mindlin plate theory to examine the buckling and post-buckling of MEE nano-plates subjected to thermal loading. Karimi *et al.* (2015) combined nonlocal refined plate theory and surface energy effects on the vibration and buckling of rectangular nano-plates using DQ method. They concluded that the nonlocal effects on vibration and shear buckling are more noticeable than that of vibration and biaxial buckling. Ansari *et al.* (2015) studied the nonlinear vibration of First shear deformation nano-plate by employing DQ method and considering surface elasticity theory. They showed that surface stress and surface elastic modulus have decreasing effect on dimensionless frequency and dimensionless amplitude; on the other hand they observed that the effect of geometrical parameters is dependent on the type of edge supports. In other work, Ansari and Gholami (2016) investigated the vibration and post-buckling behavior of third order shear deformation nano-plates considering surface elasticity theory and von Karman nonlinearity.

Functionally graded materials are novel generation of composites in which the compositions of different materials gradually change in one or multiple direction to achieve tailored properties. In most recent years, the employments of them in NEMS/MEMS have been increased (Lu, Lim and Chen 2009). Several researchers have been studied FG nano-plates subjected to mechanical and thermal loading. Zare *et al.* (2015) utilized linear methods to study the vibration response of FG nano-plates under different boundary condition based on Kirchhoff's plate theory. Using third order shear deformation plate theory, Daneshmehr *et al.* (2015) investigated the vibration behavior of embedded FG nano-plate with linear strain-displacement relations consideration. Hosseini and Jamalpoor (2017) developed a study of free vibration and buckling characteristic of FG nano-plate which is placed on visco-Pasternak foundation and found that the effect of surface layer on damped natural frequency and buckling load is dependent on the mode's degree. The effect of thermal and moisture loading on structures and nano-structures has been one of interesting subjects for many researchers (Bousahla *et al.* 2016, Bouderba *et al.* 2016, Beldjelili, Tounsi and Mahmoud 2016, El-Haina, Bousahla, Tounsi and Mahmoud 2017, Menasria, Bouhadra, Tounsi, Bousahla and Mahmoud 2017, Attia *et al.* 2018, Bouderba, Houari and Tounsi 2013, Zidi *et al.* 2014, Hamidi *et al.* 2015). In his comprehensive research, Sobhy (2015) examined bending, free vibration, mechanical and thermal buckling of FG nano-plates lying on elastic foundation; using linear strain-displacement relations, he discovered that nonlocal parameter has significant role on the variation of the stiffness of the FG nano-plates. Free vibration analysis of embedded second order FG nano-plate was presented by Panyatong *et al.* (2016), in which the nano-plate is under uniform thermal loading and simply supported boundary condition. Recently, on the basis of linear assumptions and refined plate theory, Ebrahimi and Barati (2017b) examined the influence of

environment effects (such as moisture, temperature), electric voltage and magnetic fields on vibration and buckling behavior of FG nano-plates. Inverse cotangential plate theory is employed by Barati *et al.* (2016) to study the effect of thermal loading on the buckling behavior of FG nano-plates resting on elastic foundation; they concluded that the rigidity of the plate and critical buckling temperature of the nano-plate are reduced when nonlocal parameter diminishes, however elastic foundation parameters have contrary effects on them. Nguyen *et al.* (2015) analyzed linear free vibration and buckling behavior of simply and clamped supported FG nano-plate based on Mori-Tanaka homogenization scheme and refined plate theory. Ansari *et al.* (2015) used classical plate theory to study thermal buckling and free vibration of FG nano-plate considering surface stress theory under linear temperature rise assumption. In a collaborative effort, Barati and Shahverdi (2016, 2017) investigated the thermal buckling and post-buckling and vibration responses of FG nano-plates based on refined plate theory subjected to hygro-thermal loading and different boundary conditions; in their research the linear strain-displacement relations are considered and the surface stresses are neglected.

In this research, the free vibration and buckling behavior of embedded rectangular FG nano-plates with different boundary conditions subjected to nonlinear thermal and linear moisture loading based on physical neutral surface position are studied. The material's distribution through the thickness of the plate varies as power-law function and the temperature dependent effective material properties are modeled based on Mori-Tanaka homogenization scheme. The Hamilton's principle in conjunction with Eringen nonlocal elasticity and surface elasticity theories are used to obtain governing Equations. The displacement field is based on Reddy's plate theory and nonlinear strain-displacement relations are regarded according to von Karman theory. With these assumptions the governing equations shall be solved for 5 unknowns. It can be remarked that there have been some methods which involve fewer unknowns (Belabed *et al.* 2018, Mokhtar *et al.* 2018, Houari *et al.* 2016, Hachemi *et al.* 2017, Mouffoki *et al.* 2017), but they often comprise assumptions that make them appropriate for linear approaches. GDQ method, as an efficient numerical method to solve complicated partial and ordinary differential equations (Shu 2012), in conjunction with Iterative method is used to solve the governing equations. Finally, the effect of nonlocal parameter, volume fraction exponent, geometrical parameters, elastic foundation parameters, surface parameters, thermal and moisture loading on natural frequencies and critical buckling load are depicted. A comparison study with the results of hyperbolic shear deformation plate theory is available in this article.

2. Theory

Consider a rectangular ceramic- metal FG nano-plate of thickness h , length a and width b resting on a Pasternak elastic foundation with Winkler (K_w) and Pasternak (K_p) modulus as shown in Fig. 1. Noting that the material at the top surface ($z = \frac{h}{2}$) is ceramic-rich and the bottom surface ($z = -\frac{h}{2}$) is metal-rich the following theories are simultaneously remarked.

2.1 Nonlocal constitutive formulation

In contrast to the classical elasticity theory, the stress at a specified point like x is supposed to be a function of the strain components at all other points of the body (Eringen 1983, 1972).

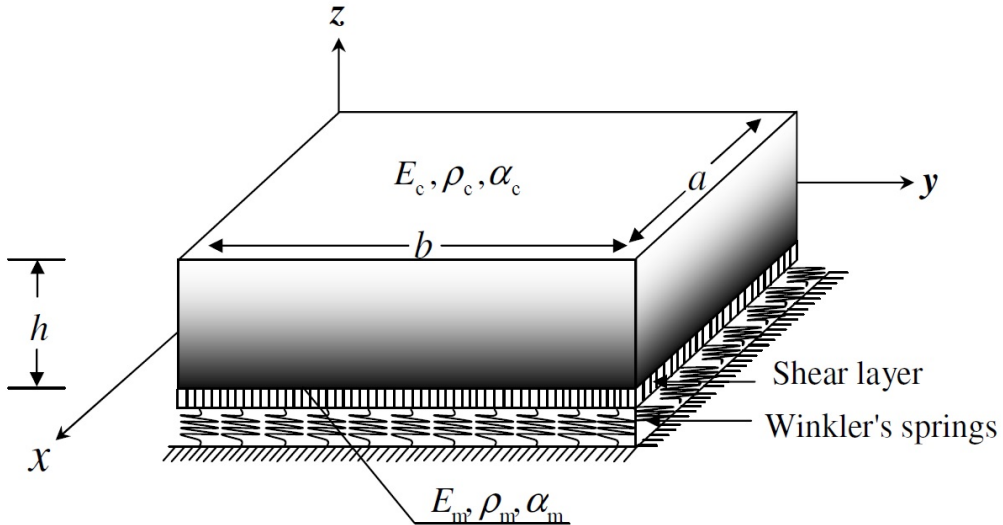


Fig. 1 Geometry of a rectangular FG nano-plate resting on Pasternak elastic foundation (Sobhy 2015).

According to nonlocal elasticity theory, the constitutive relation can be stated as:

$$\sigma_{ij}^{nl}(x) = \int_V \alpha(|x' - x|, \tau) \sigma_{ij}^d(x') dv(x'), \quad (1.1)$$

$$\sigma_{ij}^d(x') = C_{ijkl} \varepsilon_{kl}(x') \quad (1.2)$$

where $\sigma_{ij}^{nl}(x)$ is nonlocal stress at the point x , $\sigma_{ij}^d(x')$ is the classical stress at any point x' in the body with volume function $v(x')$, $\alpha(|x' - x|, \tau)$ is nonlocal modulus and also Green's function, $\varepsilon_{kl}(x')$ and C_{ijkl} are strain and the fourth-order elasticity tensor respectively. By neglecting the effects of strains at points other than reference point x , one can obtain classical elasticity theory. From Green's function theory (Duffy 2015), Eq. (1.1) can be rewritten as:

$$(1 - \mu \nabla^2) \sigma_{ij}^{nl} = \sigma_{ij}^d, \quad (2)$$

where

$$\mathbf{L} = 1 - \mu \nabla^2, \quad (3)$$

is the corresponding differential operator for two-dimensional nonlocal modulus, μ is nonlocal parameter and ∇^2 is the Laplacian operator.

2.2 Surface elasticity model

When sizes of structures are greater than 50 nm, usually, the surface-to-volume ratio is negligible and classical constitutive relations dominate the deformation behavior of the structure (Shahram, Ganti, Ardebili and Alizadeh, 2004). However, for smaller sizes the role of surface increases and classical constitutive relations shall be replaced with appropriate equations. Meanwhile, one deals with terminologies such as "surface energy" and "surface stress"; but, it should be noted that the concepts of these terminologies can be very different, specially, about

solids. The surface energy is defined as a reversible work per unit area to form a surface. This quantity is always positive and then unstable; this means the solid would lose energy upon fragmentation. On the other hand, the surface stress is defined as a reversible work per area to stretch a surface elastically. Unlike the surface energy, surface stress can be positive or negative. For a liquid, the surface stress and surface energy are equal they are frequently referred to by the common name “surface tension”. Mathematically, the surface stress is defined as (Ibach 1997):

$$S_{\bar{j}} = \int_{-\infty}^{+\infty} (\sigma_{\bar{j}}(z) - \sigma_{\bar{j}}^b) dz, \quad (4)$$

where $S_{\bar{j}}$ is the component of the surface stress tensor, $\sigma_{\bar{j}}(z)$ considered as bulk stress tensor components and $\sigma_{\bar{j}}^b$ is the residual surface stress tensor component.

The constitutive relation regarding surface stress is obtained by Gurtin and Murdoch (Gurtin and Murdoch 1975, Gurtin and Murdoch 1978) as:

$$\frac{\partial S_{\bar{j}}}{\partial x_j} = \sigma_{\bar{j}} n_j + \rho_0 \ddot{u}_i \quad i, j = x, y, z, \quad (5.1)$$

$$S_{\bar{j}} = \tau_0 \delta_{\bar{j}} + 2(\mu_0 - \tau_0) E_{\bar{j}} + (\lambda_0 + \tau_0) E_{kk} \delta_{\bar{j}} + \tau_0 \frac{\partial u_i}{\partial x_j} + o(\varepsilon) \quad (5.2)$$

$$S_{\bar{i}} = \tau_0 \frac{\partial u_z}{\partial x_i} \quad i, j = x, y \quad (5.3)$$

the above relations are valid where $\rho_0, \tau_0, \lambda_0$ and μ_0 represent mass density, residual stress and Lame moduli of the surface, n_j denotes normal to surface, u_i and x_j are displacement and coordinate in the i and j directions and $\sigma_{\bar{j}}$ is bulk stress tensor; all nonlinear components are considered in $o(\varepsilon)$.

Herein, Eqs. (5.1)-(5.3) will be used to calculate strain energy due to surface stresses but it shouldn't be neglected that surface stresses alter the distribution of stresses in the z direction (σ_z^{nl}); however, this distribution is such that the average of distribution function ($\bar{f}(z)$) is vanished :

$$0 = \frac{\int_{-\frac{h}{2}}^{\frac{h}{2}} \bar{f}(z) dz}{h}, \quad (6)$$

where h is the thickness of the plate.

Using distribution function ($\bar{f}(z)$), and considering nonlocal elasticity theory, one can write the nonlocal stress in z direction as:

$$\begin{aligned} \sigma_z^{nl} &= \bar{f}(z) \{ (\tau_0^+ + \tau_0^-)(w_{,xx} + w_{,yy} - (\rho_0^- + \rho_0^+) \ddot{w}) \} \\ &\quad + \frac{1}{2} \{ (\tau_0^+ - \tau_0^-)(w_{,xx} + w_{,yy} + (\rho_0^- - \rho_0^+) \ddot{w}) \}, \end{aligned} \quad (7)$$

where w denotes the displacement in z direction.

Eq. (7) is used in classical constitutive relation:

$$\sigma_{\bar{j}}^d = \frac{E}{1+v} \left(\varepsilon_{\bar{j}} + \frac{v}{1-v} \varepsilon_{kk} \delta_{\bar{j}} \right) + \frac{v}{1-v} \sigma_z^d \delta_{\bar{j}} \quad (8)$$

after applying the nonlocal differential operator (Eq. 3). In this equation E is Young's modulus, and ν Poisson's ratio.

In this article we assume:

$$\bar{f}(z) = \frac{z}{h} \quad (9)$$

2.3 Higher order shear deformation plate theory

The displacement field for a plate in HSDT can be described in a general form by (Gholami, Ansari and Gholami 2017):

$$u(x, y, z, t) = u_0(x, y, t) - f(z)\varphi_x(x, y, t) + (f(z) - z)w_{0,x}(x, y, t) \quad (10.1)$$

$$v(x, y, z, t) = v_0(x, y, t) - f(z)\varphi_y(x, y, t) + (f(z) - z)w_{0,y}(x, y, t) \quad (10.2)$$

$$w(x, y, z, t) = w_0(x, y, t) \quad (10.3)$$

In the above equations (u, v, w) are displacements of any point of the nano-plate in (x, y, z) directions; (u_0, v_0, w_0) are the displacement components of the mid-plane at time t. φ_x and φ_y denotes the rotation of a transverse normal about the y and x axis. $f(z)$ is the unified kinematic function which characterizes the transverse shear deformation and stress distribution through the thickness of the nano-plate. In terms of $f(z)$ there are different plate theories, for example if $f(z) = 0$ we have Krichhoff plate theory or if $f(z) = z$ the plate theory is Mindlin plate theory. In the present research the Reddy and Hyperbolic shear deformation plate theory are studied where:

$$f(z) = z(1 - \frac{4z^2}{3h^2}) \quad \text{for Reddy plate theory} \quad (11.1)$$

$$f(z) = h \sinh\left(\frac{z}{h}\right) - z \cosh\left(\frac{1}{2}\right) \quad \text{for Hyperbolic shear deformation plate theory} \quad (11.2)$$

2.4 Mori-Tanaka FGM plate model considering the physical neutral surface

Consider the distribution of material in the FG nano-plate changes through the thickness as power-law function:

$$V_c = \left(\frac{1}{2} + \frac{z}{h}\right)^p \quad (12.1)$$

$$V_c + V_m = 1 \quad (12.2)$$

where $0 \leq V_c, V_m \leq 1$ are respectively the volume fraction of ceramic and metal at point (x, y, z) and p is the volume fraction exponent.

The effective material properties can be calculated using Mori-Tanaka homogenization scheme (Shen 2016):

$$\frac{K_f(z, T) - K_c(T)}{K_m(T) - K_c(T)} = \frac{V_m}{1 + (1 - V_m)(3(K_m(T) - K_c(T))/(3K_c(T) + 4G_c(T)))} \quad (13.1)$$

$$\frac{G_f(z, T) - G_c(T)}{G_m(T) - G_c(T)} = \frac{V_m}{1 + (1 - V_m)((G_m(T) - G_c(T))/(G_c(T) + f_c))} \quad (13.2)$$

$$\frac{\alpha_f(z, T) - \alpha_c(T)}{\alpha_m(T) - \alpha_c(T)} = \frac{\frac{1}{K_f(z, T)} - \frac{1}{K_c(T)}}{\frac{1}{K_m(T)} - \frac{1}{K_c(T)}} \quad (13.3)$$

$$\frac{\kappa_f(z, T) - \kappa_c(T)}{\kappa_m(T) - \kappa_c(T)} = \frac{V_m}{1 + (1 - V_m)((\kappa_m(T) - \kappa_c(T))/3\kappa_c(T))} \quad (13.4)$$

$$f_c = \frac{G_c(T)(9K_c(T) + 8G_c(T))}{6(K_c(T) + 2G_c(T))} \quad (13.5)$$

in above relations K is effective bulk modulus, G is effective shear modulus, α is considered as effective thermal expansion coefficient and κ regarded as effective thermal conductivity; all material properties are temperature (T) dependent and the subscripts "m", "c" and "f" are metal, ceramic and effective property.

The effective density of material is obtained based on the rule of mixture relation (Qian, Batra and Chen 2004):

$$\rho_c V_c + \rho_m V_m = \rho_f \quad (14)$$

Since in FG plates there is no mid-plane symmetry condition, the stretching equation is coupled with bending equation, while kinematic relations are symmetric; to solve this discrepancy the neutral surface of the plate is selected as the origin of the coordinate system and the variable z changes to $(z - z_0)$ where z_0 is the elevation of neutral surface and is calculated as (Zhang and Zhou 2008):

$$z_0 = \frac{\int_{-\frac{h}{2}}^{\frac{h}{2}} z E(z) dz}{\int_{-\frac{h}{2}}^{\frac{h}{2}} E(z) dz} \quad (15)$$

2.5 Thermal effect

At first glance, temperature rising affects the properties of material. In cases where there is no explicit relation for temperature dependent material properties, the curve fitting methods (Ahn 2004) and data from tables can be used to model aforesaid effect as polynomial (Reddy J. N. 2011):

$$P = P_0(P_{-1}T^{-1} + 1 + P_1T + P_2T^2 + P_3T^3) \quad (16)$$

where P is typical material property, P_0, P_{-1}, P_1, P_2 and P_3 are the coefficients of temperature.

Temperature variation can also expand or contract the material and in the result thermal stresses are developed. If v and α are Poisson's ratio and coefficient of thermal expansion (CTE), the classical thermal constitutive equation for an isotropic material in two-dimensional space can be

written as (Shen 2016, Bloom and Coffin 2000, Reddy J. N. 2006):

$$\sigma_x^T = \sigma_y^T = \frac{E}{1-v} \alpha \Delta T \quad \sigma_{xy}^T = 0 \quad (17)$$

where σ_x^T , σ_y^T and σ_{xy}^T are thermal stresses in the material.

2.6 Moisture effect

The moisture absorption has analogous effect to temperature on developed stresses in material (Marie 2012); the stresses due to moisture variation are calculated as:

$$\sigma_x^C = \sigma_y^C = \frac{E}{1-v} \beta \Delta C \quad \sigma_{xy}^C = 0 \quad (18)$$

For a material of mass "m", C (the relative mass moisture concentration) can be calculated as (Vasiliev and Morozov 2013):

$$C = \frac{\Delta m}{m} \quad (19)$$

where Δm is mass increase after moisture absorption.

In Eq. (18), β is coefficient of moisture expansion (CME) and considered to be constant through the thickness.

The moisture absorption by metal is neglected in the present paper and it is assumed that the amount of β and C are around the ceramic tiles values (Link International 2016):

$$\beta = 60 \text{ mm/m} \quad C = 3\text{--}6\% \quad (20)$$

2.7 Temperature and moisture field

The temperature and moisture field is assumed to be constant in the XY plane of the plate. Eqs. (21)-(22) is used to calculate temperature and moisture field (Vasiliev and Morozov 2013, Javaheri and Eslami 2002):

$$\frac{d}{dz} \left[\kappa_f(z, T) \frac{dT}{dz} \right] = 0 \quad (21)$$

$$\frac{d}{dz} \left(D(z, T) \frac{dC}{dz} \right) = 0 \quad (22)$$

where $D(z, T)$ is diffusion coefficient.

Using Eq. (21) the nonlinear temperature rise can be calculated as:

$$\Delta T = T(z) - T_0 = (T_m - T_0) + \Delta T_{cn} \frac{\int_{-\frac{h}{2}}^z \frac{dz}{\kappa_f(z, T)}}{\int_{-\frac{h}{2}}^{h/2} \frac{dz}{\kappa_f(z, T)}} \quad \text{where} \quad \Delta T_{cn} = T_c - T_m \quad (23)$$

For linear moisture concentration rise from Eq. (22) we have:

$$\Delta C = C(z) - C_0 = (C_m - C_0) + \Delta C_{cn} \frac{(z + h/2)}{h} \quad \text{where} \quad \Delta C_{cn} = C_c - C_m \quad (24)$$

where T_0 and C_0 are initial temperature and initial moisture concentration.

3. Free vibration Analysis

For a system at dynamic equilibrium the governing equation can be driven using Hamilton's principle (Reddy J. N. 2006):

$$0 = \int_0^{t_0} (\delta U + \delta V - \delta K) dt \quad (25)$$

The variation of strain energy in Hamilton's principle (δU) can be written as:

$$\delta U = \delta U_b + \delta U_s \quad (26)$$

where (Reddy J. N. 2011, Ansari *et al.* 2014):

$$\delta U_b = \int_{\Omega} \int_{-\frac{h}{2}}^{\frac{h}{2}} (\sigma_{xx}^{nl} \delta \varepsilon_{xx} + \sigma_{yy}^{nl} \delta \varepsilon_{yy} + 2\sigma_{xy}^{nl} \delta \varepsilon_{xy} + 2\sigma_{xz}^{nl} \delta \varepsilon_{xz} + 2\sigma_{yz}^{nl} \delta \varepsilon_{yz}) dz dx dy \quad (27.1)$$

$$\begin{aligned} \delta U_s &= \delta U_s^+ + \delta U_s^- \\ &= \int_{\Lambda} \left((S_{xx}^{nl+} + S_{xx}^{nl-}) \delta \varepsilon_{xx} + (S_{xy}^{nl+} + S_{yx}^{nl+} + S_{xy}^{nl-} + S_{yx}^{nl-}) \delta \varepsilon_{xy} \right. \\ &\quad + (S_{yy}^{nl+} + S_{yy}^{nl-}) \delta \varepsilon_{yy} + 2 \left((S_{xz}^{nl+} + S_{xz}^{nl-}) \right) \delta \varepsilon_{xz} \\ &\quad \left. + 2(S_{yz}^{nl+} + S_{yz}^{nl-}) \delta \varepsilon_{yz} \right) dx dy \end{aligned} \quad (27.2)$$

where “+”, “-”, b and s denote top surface, bottom surface, body and surface of the nano-plate; Ω and Λ are the undeformed middle plane of the plate and the undeformed surface layer of the plate.

To calculate the variation of work due to external forces and environment interactions (δV) in Eq. (25) we have (Reddy J. N. 2006, Praveen and Reddy 1998):

$$\delta V = \delta V^T + \delta V^c + \delta V^e \quad (28)$$

where:

$$\delta V^T = - \int_{\Omega} \int_{-\frac{h}{2}}^{\frac{h}{2}} \sigma_{ij}^{T,nl} \delta \varepsilon_{ij} dz dx dy = - \int_{\Omega} \int_{-\frac{h}{2}}^{\frac{h}{2}} (\sigma_x^{T,nl} \delta \varepsilon_x + \sigma_y^{T,nl} \delta \varepsilon_y) dz dx dy \quad (29.1)$$

$$\delta V^c = - \int_{\Omega} \int_{-\frac{h}{2}}^{\frac{h}{2}} \sigma_{ij}^{c,nl} \delta \varepsilon_{ij} dz dx dy = - \int_{\Omega} \int_{-\frac{h}{2}}^{\frac{h}{2}} (\sigma_x^{c,nl} \delta \varepsilon_x + \sigma_y^{c,nl} \delta \varepsilon_y) dz dx dy \quad (29.2)$$

$$\begin{aligned} \delta V^e = - \int_{\Omega} (q - K_w w_0 + K_p \nabla^2 w_0) \delta w_0 \, dx \, dy \\ - \int_{\Gamma_\sigma} \left(\hat{N}_{nn} \delta u_{0n} + \hat{M}_{nn} \delta \varphi_n - \frac{4}{3h^2} \hat{P}_{nn} \delta \psi_n + \hat{N}_{ns} \delta u_{0s} + \hat{M}_{ns} \delta \varphi_s \right. \\ \left. - \frac{4}{3h^2} \hat{P}_{ns} \delta \psi_s + \hat{Q}_n \delta w_0 \right) d\Gamma \end{aligned} \quad (29.3)$$

where, V^T, V^c and V^e are, respectively, work due to thermal stresses, due to moisture stresses and external forces; $q(x, y)$ is resultant of distributed transverse loads applied at the upper and lower surface of the nano-plate; $\hat{\sigma}_{nn}$, $\hat{\sigma}_{ns}$ and $\hat{\sigma}_{nz}$ are stresses acting on the portion Γ_σ of the boundary of the plate; the effect of foundation can be found by changing Winkler modulus (K_w) and Pasternak modulus (K_p) parameters (Jung, Park and Han 2014); for resultant stresses in Eq. (29.3) we have:

$$\begin{Bmatrix} \hat{N}_{\bar{j}} \\ \hat{M}_{\bar{j}} \\ \hat{P}_{\bar{j}} \end{Bmatrix} = \int_{-\frac{h}{2}}^{\frac{h}{2}} \hat{\sigma}_{\bar{j}} \begin{Bmatrix} 1 \\ z \\ z^3 \end{Bmatrix} dz \quad \hat{Q}_n = \int_{-\frac{h}{2}}^{\frac{h}{2}} \hat{\sigma}_{nz} dz \quad \hat{Q}_n = \int_{-\frac{h}{2}}^{\frac{h}{2}} \hat{\sigma}_{nz} dz \quad (30)$$

The strains are related to displacement variables according to von Karman's theory:

$$\begin{cases} \varepsilon_{\bar{j}} = \varepsilon_{\bar{j}}^0 + z \varepsilon_{\bar{j}}^{(1)} - z^3 \varepsilon_{\bar{j}}^{(3)} & i, j = x, y \\ \varepsilon_{\bar{j}} = \varepsilon_{\bar{j}}^0 + z^2 \varepsilon_{\bar{j}}^{(2)} & i = x, y; j = z \end{cases} \quad (31)$$

where:

$$\begin{aligned} \varepsilon_{xx}^0 &= \frac{1}{2} \left(\frac{\partial w_0}{\partial x} \right)^2 + \frac{\partial u_0}{\partial x} & \varepsilon_{xx}^{(1)} &= \frac{\partial \varphi_x}{\partial x} & \varepsilon_{xx}^{(3)} &= \frac{4}{3h^2} \left(\frac{\partial \varphi_x}{\partial x} + \frac{\partial^2 w_0}{\partial x^2} \right) \\ \varepsilon_{yy}^0 &= \frac{1}{2} \left(\frac{\partial w_0}{\partial y} \right)^2 + \frac{\partial v_0}{\partial y} & \varepsilon_{yy}^{(1)} &= \frac{\partial \varphi_y}{\partial y} & \varepsilon_{yy}^{(3)} &= \frac{4}{3h^2} \left(\frac{\partial \varphi_y}{\partial y} + \frac{\partial^2 w_0}{\partial y^2} \right) \\ \varepsilon_{xy}^0 &= \frac{1}{2} \left(\frac{\partial u_0}{\partial y} + \frac{\partial v_0}{\partial x} + \frac{\partial w_0}{\partial x} \frac{\partial w_0}{\partial y} \right) & \varepsilon_{xy}^{(1)} &= \frac{1}{2} \left(\frac{\partial \varphi_x}{\partial y} + \frac{\partial \varphi_y}{\partial x} \right) & \varepsilon_{xy}^{(3)} &= \frac{2}{3h^2} \left(\frac{\partial \varphi_x}{\partial y} + \frac{\partial \varphi_y}{\partial x} \right) \\ &&&&&+ \frac{4}{3h^2} \frac{\partial^2 w_0}{\partial x \partial y} \end{aligned} \quad (32)$$

$$\begin{aligned} \varepsilon_{xz}^0 &= \frac{1}{2} \left(\varphi_x + \frac{\partial w_0}{\partial x} \right) & \varepsilon_{xz}^{(2)} &= -\frac{2}{h^2} \left(\varphi_x + \frac{\partial w_0}{\partial x} \right) \\ \varepsilon_{yz}^0 &= \frac{1}{2} \left(\varphi_y + \frac{\partial w_0}{\partial y} \right) & \varepsilon_{yz}^{(2)} &= -\frac{2}{h^2} \left(\varphi_y + \frac{\partial w_0}{\partial y} \right) \end{aligned}$$

The variation of the kinetic energy (δK) in Hamilton's principle Eq. (25) can be derived as (Reddy J. N. 2006):

$$\begin{aligned} \delta K = \int_{\Omega} \left\{ & \left(I_0 \dot{u}_0 + I_1 \dot{\phi}_x - \frac{4I_3}{3h^2} \dot{\psi}_x \right) \delta \dot{u}_0 + \left(I_0 \dot{v}_0 + I_1 \dot{\phi}_y - \frac{4I_3}{3h^2} \dot{\psi}_y \right) \delta \dot{v}_0 \right. \\ & + \left(I_1 \dot{u}_0 + I_2 \dot{\phi}_x - \frac{4I_4}{3h^2} \dot{\psi}_x \right) \delta \dot{\phi}_x + \left(-\frac{4I_3}{3h^2} \dot{u}_0 - \frac{4I_4}{3h^2} \dot{\phi}_x + \frac{16I_6}{9h^4} \dot{\psi}_x \right) \delta \dot{\psi}_x \\ & + \left(I_1 \dot{v}_0 + I_2 \dot{\phi}_y - \frac{4I_4}{3h^2} \dot{\psi}_y \right) \delta \dot{\phi}_y + \left(-\frac{4I_3}{3h^2} \dot{v}_0 - \frac{4I_4}{3h^2} \dot{\phi}_y + \frac{16I_6}{9h^4} \dot{\psi}_y \right) \delta \dot{\psi}_y \\ & \left. + I_0 \dot{w}_0 \delta \dot{w}_0 \right\} dx dy \end{aligned} \quad (33)$$

where:

$$I_i = \int_{-\frac{h}{2}}^{\frac{h}{2}} \rho z^i dz \quad \psi_j = \varphi_j - z \frac{\partial w_0}{\partial j} \quad \delta \psi_j = \delta \varphi_j - z \frac{\partial \delta w_0}{\partial j} \quad (34)$$

Using Eqs. (25)-(34), the governing equations can be obtained as:

$$\delta u_0: \quad \bar{N}_{xx,x} + \bar{N}_{xy,y} = I_0 \mathbf{L} \ddot{u}_0 - I_{13} \mathbf{L} \ddot{\phi}_x - \frac{4I_3}{3h^2} \mathbf{L} \ddot{w}_{0,x} \quad (35.1)$$

$$\delta v_0: \quad \bar{N}_{yy,y} + \bar{N}_{xy,x} = I_0 \mathbf{L} \ddot{v}_0 - I_{13} \mathbf{L} \ddot{\phi}_y - \frac{4I_3}{3h^2} \mathbf{L} \ddot{w}_{0,y} \quad (35.2)$$

$$\delta \varphi_x: \quad -\bar{M}_{xx,x} - \bar{M}_{xy,y} + \frac{4}{3h^2} (\bar{P}_{xx,x} + \bar{P}_{xy,y}) + \bar{Q}'_x = I_{13} \mathbf{L} \ddot{u}_0 + I_{246} \mathbf{L} \ddot{\phi}_x + I_{46} \mathbf{L} \ddot{w}_{0,x} \quad (35.3)$$

$$\delta \varphi_y: \quad -\bar{M}_{yy,y} - \bar{M}_{xy,x} + \frac{4}{3h^2} (\bar{P}_{yy,y} + \bar{P}_{xy,x}) + \bar{Q}'_y = I_{13} \mathbf{L} \ddot{v}_0 + I_{246} \mathbf{L} \ddot{\phi}_y + I_{46} \mathbf{L} \ddot{w}_{0,y} \quad (35.4)$$

$$\begin{aligned} \delta w_0: & -\frac{4}{3h^2} (\bar{P}_{xx,xx} + \bar{P}_{yy,yy} + 2\bar{P}_{xy,xy}) - \mathbf{L} (\bar{N}^{nl}(u_0, v_0, w_0)) - \bar{Q}'_{x,x} - \bar{Q}'_{y,y} \\ & - K_p \mathbf{L} \nabla^2 w_0 + K_w \mathbf{L} w_0 \\ & = -I_0 \mathbf{L} \ddot{w}_0 - \frac{4I_3}{3h^2} (\mathbf{L} \ddot{u}_{0,x} + \mathbf{L} \ddot{v}_{0,y}) - I_{46} (\mathbf{L} \ddot{\phi}_{x,x} + \mathbf{L} \ddot{\phi}_{y,y}) \\ & + \frac{16I_6}{9h^4} \mathbf{L} \nabla^2 \ddot{w}_0 \end{aligned} \quad (35.5)$$

with boundary condition as:

$$\delta u_{0n} = 0 \quad \text{or} \quad \bar{N}_{nn} = \hat{N}_{nn} \quad (36.1)$$

$$\delta u_{0s} = 0 \quad \text{or} \quad \bar{N}_{ns} = \hat{N}_{ns} \quad (36.2)$$

$$\delta w_0 = 0 \quad \text{or} \quad \bar{V}_n = \hat{V}_n \quad (36.3)$$

$$\delta \varphi_n = 0 \quad \text{or} \quad \bar{M}_{nn} - \frac{4}{3h^2} \bar{P}_{nn} = \hat{M}_{nn} - \frac{4}{3h^2} \hat{P}_{nn} \quad (36.4)$$

$$\delta\varphi_s = 0 \quad \text{or} \quad \bar{M}_{ns} - \frac{4}{3h^2} \bar{P}_{ns} = \hat{M}_{ns} - \frac{4}{3h^2} \hat{P}_{ns} \quad (36.5)$$

$$\frac{\partial \delta w_0}{\partial n} = 0 \quad \text{or} \quad \bar{P}_{nn} = \hat{P}_{nn} \quad (36.6)$$

where:

$$\bar{N}^{nl}(u_0, v_0, w_0) = (\bar{N}_{xx}^{nl} w_{0,x} + \bar{N}_{xy}^{nl} w_{0,y})_{,x} + (\bar{N}_{yy}^{nl} w_{0,y} + \bar{N}_{yx}^{nl} w_{0,x})_{,y} \quad (37.1)$$

$$\bar{A}_{\bar{j}} = A_{\bar{j}} + A_{\bar{j}}^s - A_{\bar{j}}^T - A_{\bar{j}}^c \quad A = N, M, P \quad i = x, y \quad (37.2)$$

$$[N_{\bar{j}}, M_{\bar{j}}, P_{\bar{j}}] = \int_{-\frac{h}{2}}^{\frac{h}{2}} \sigma_{\bar{j}} [1, z, z^3] dz \quad i = x, y \quad (37.3)$$

$$[N_{\bar{j}}^\zeta, M_{\bar{j}}^\zeta, P_{\bar{j}}^\zeta] = \int_{-\frac{h}{2}}^{\frac{h}{2}} \sigma_{\bar{j}}^\zeta [1, z, z^3] dz \quad \zeta = c, T \quad (37.4)$$

$$\bar{A}_i = A_i + A_i^s \quad A = Q, R \quad \bar{Q}'_i = \bar{Q}_i - \frac{4\bar{R}_i}{h^2} \quad i = x, y \quad (37.5)$$

$$[Q_i, R_i] = \int_{-\frac{h}{2}}^{\frac{h}{2}} \sigma_{\bar{i}} [1, z^2] dz \quad i = x, y \quad (37.6)$$

$$\begin{Bmatrix} N_{\bar{j}}^s \\ M_{\bar{j}}^s \\ P_{\bar{j}}^s \end{Bmatrix} = \begin{Bmatrix} \frac{(S_{\bar{j}}^+ + S_{\bar{j}}^- + S_{\bar{j}}^- + S_{\bar{j}}^-)}{2} \\ \frac{(S_{\bar{j}}^+ + S_{\bar{j}}^- - S_{ij}^- - S_{\bar{j}}^-)}{4} \frac{h}{4} \\ \frac{(S_{\bar{j}}^+ + S_{\bar{j}}^- - S_{\bar{j}}^- - S_{\bar{j}}^-)}{2} \left(\frac{h}{2}\right)^3 \end{Bmatrix} \quad \begin{Bmatrix} Q_i^s \\ R_i^s \end{Bmatrix} = \begin{Bmatrix} S_{\bar{i}}^+ + S_{\bar{i}}^- \\ (S_{\bar{i}}^+ + S_{\bar{i}}^-) \left(\frac{h}{2}\right)^2 \end{Bmatrix} \quad (37.7)$$

$$\hat{V}_n = \hat{Q}_n + \frac{4}{3h^2} \frac{\partial \hat{P}_{ns}}{\partial s} \quad \hat{Q}_n = \int_{-\frac{h}{2}}^{\frac{h}{2}} \hat{\sigma}_{nz} dz \quad (37.8)$$

$$\bar{V}_n = \mathbf{L} \bar{V}_n^{nl} \quad (37.9)$$

$$\begin{aligned} \bar{V}_n^{nl} &= P^{nl}(u_0, v_0, w_0) + \frac{4}{3h^2} (\bar{P}_{xx,x}^{nl} + \bar{P}_{xy,y}^{nl}) n_x + \frac{4}{3h^2} (\bar{P}_{yy,y}^{nl} + \bar{P}_{xy,x}^{nl}) n_y + \bar{Q}_x^{nl} n_x + \bar{Q}_y^{nl} n_y \\ &\quad - \left(I_{46} \ddot{\varphi}_y - \frac{16I_6}{9h^4} \ddot{w}_{0,y} \right) n_y - \left(I_{46} \ddot{\varphi}_x - \frac{16I_6}{9h^4} \ddot{w}_{0,x} \right) n_x - \frac{4I_3}{3h^2} \ddot{u}_0 n_x \\ &\quad - \frac{4I_3}{3h^2} \ddot{v}_0 n_y + \frac{4}{3h^2} \frac{\partial \bar{P}_{ns}^{nl}}{\partial s} \end{aligned} \quad (37.10)$$

$$I_{13} = \frac{4I_3}{3h^2} - I_1 \quad I_{246} = -I_2 + \frac{8I_4}{3h^2} - \frac{16I_6}{9h^4} \quad I_{46} = \frac{4I_4}{3h^2} - \frac{16I_6}{9h^4} \quad (37.11)$$

Linearizing of Eq. (37.1) gives (Reddy J. N. 2010):

$$\bar{N}^{nl}(u_0, v_0, w_0) \approx \bar{N}_{xx}^{nl}w_{0,xx} + 2\bar{N}_{xy}^{nl}w_{0,xy} + \bar{N}_{yy}^{nl}w_{0,yy} \quad (38)$$

In the result we can write:

$$\mathbf{L}\left(\bar{N}^{nl}(u_0, v_0, w_0)\right) \approx \bar{N}_{xx}w_{0,xx} + 2\bar{N}_{xy}w_{0,xy} + \bar{N}_{yy}w_{0,yy} \quad (39)$$

Since all non-homogeneous parts are negligible the governing Equations (Eqs. (35.1)-(35.5)) can be solve with following change of variables:

$$\begin{Bmatrix} u_0(x, y, t) \\ v_0(x, y, t) \\ w_0(x, y, t) \\ \varphi_x(x, y, t) \\ \varphi_y(x, y, t) \end{Bmatrix} = \begin{Bmatrix} U_0(x, y) \\ V_0(x, y) \\ W_0(x, y) \\ \Phi_x(x, y) \\ \Phi_y(x, y) \end{Bmatrix} e^{j\omega t} \quad (40)$$

4. Buckling Analysis

The governing buckling equations are obtained from (Jones 2006):

$$\delta^2\Pi|_{\delta\Pi=0}(\text{static situation}) = 0 \quad (41)$$

where Π is the total potential energy:

$$\Pi = U + V - K \quad (42)$$

From strain-stress relations we have ($K = 0$):

$$\begin{aligned} \delta^2\Pi = & \int_{\Omega} \int_{-\frac{h}{2}}^{\frac{h}{2}} \{ [(-\bar{N}_{xx,x}^{nl} - \bar{N}_{xy,y}^{nl})\delta^2u_0 + (-\bar{N}_{yy,y}^{nl} - \bar{N}_{xy,x}^{nl})\delta^2v_0 + (-\bar{M}_{xx,x}^{nl} - \bar{M}_{xy,y}^{nl} + \\ & + \frac{4}{3h^2}(\bar{P}_{xx,x}^{nl} + \bar{P}_{xy,y}^{nl}) + \bar{Q}'_x^{nl})\delta^2\varphi_x + (-\bar{M}_{yy,y}^{nl} - \bar{M}_{xy,x}^{nl} + \frac{4}{3h^2}(\bar{P}_{yy,y}^{nl} + \bar{P}_{xy,x}^{nl}) + \\ & + \bar{Q}'_y^{nl})\delta^2\varphi_y + (-\frac{4}{3h^2}(\bar{P}_{xx,xx}^{nl} + \bar{P}_{yy,yy}^{nl} + 2\bar{P}_{xy,xy}^{nl}) - \\ & - (\bar{N}_{xx}^{nl}w_{0,x} + \bar{N}_{xy}^{nl}w_{0,y})_x - (\bar{N}_{yy}^{nl}w_{0,y} + \bar{N}_{xy}^{nl}w_{0,x})_y - \bar{Q}'_{x,x}^{nl} - \bar{Q}'_{y,y}^{nl} - K_p\nabla^2w_0 + \\ & + K_w w_0)\delta^2w_0 + \bar{N}_{xx}^{nl}\delta w_{0,x}^2 + 2\bar{N}_{xy}^{nl}\delta w_{0,x}\delta w_{0,y} + \bar{N}_{yy}^{nl}\delta w_{0,y}^2] + \\ & + [(-\delta\bar{N}_{xx,x}^{nl} - \delta\bar{N}_{xy,y}^{nl})\delta u_0 + (-\delta\bar{N}_{yy,y}^{nl} - \delta\bar{N}_{xy,x}^{nl})\delta v_0 + (-\delta\bar{M}_{xx,x}^{nl} - \delta\bar{M}_{xy,y}^{nl} + \\ & + \frac{4}{3h^2}(\delta\bar{P}_{xx,x}^{nl} + \delta\bar{P}_{xy,y}^{nl}) + \delta\bar{Q}'_x^{nl})\delta\varphi_x + (-\delta\bar{M}_{yy,y}^{nl} - \delta\bar{M}_{xy,x}^{nl} + \frac{4}{3h^2}(\delta\bar{P}_{yy,y}^{nl} + \\ & + \delta\bar{P}_{xy,x}^{nl}) + \delta\bar{Q}_y^{nl})\delta\varphi_y + (-\frac{4}{3h^2}(\delta\bar{P}_{xx,xx}^{nl} + \delta\bar{P}_{yy,yy}^{nl} + 2\delta\bar{P}_{xy,xy}^{nl}) - \end{aligned} \quad (43)$$

$$\begin{aligned}
& -(\delta \bar{N}_{xx}^{nl} w_{0,x} + \delta \bar{N}_{xy}^{nl} w_{0,y})_{,x} - (\delta \bar{N}_{yy}^{nl} w_{0,y} + \delta \bar{N}_{xy}^{nl} w_{0,x})_{,y} - K_p \nabla^2 \delta w_0 + \\
& + K_w \delta w_0 - \delta \bar{Q}'_{x,x}^{nl} - \delta \bar{Q}'_{y,y}^{nl}] \} \delta w_0 \, dx \, dy + \\
& + \oint_{\Gamma} \{ [(\bar{N}_{xx}^{nl} nx + \bar{N}_{xy}^{nl} ny) \delta^2 u_0 + (\bar{N}_{xy}^{nl} nx + \bar{N}_{yy}^{nl} ny) \delta^2 v_0 + (\left(\bar{M}_{xx}^{nl} - \frac{4 \bar{P}_{xx}^{nl}}{3h^2} \right) nx + \\
& + \left(\bar{M}_{xy}^{nl} - \frac{4 \bar{P}_{xy}^{nl}}{3h^2} \right) ny) \delta^2 \varphi_x + \left(\left(\bar{M}_{yy}^{nl} - \frac{4 \bar{P}_{yy}^{nl}}{3h^2} \right) ny + \left(\bar{M}_{xy}^{nl} - \frac{4 \bar{P}_{xy}^{nl}}{3h^2} \right) nx \right) \delta^2 \varphi_y + \\
& + (\frac{4}{3h^2} (\bar{P}_{xx,x}^{nl} + \bar{P}_{xy,y}^{nl}) nx + \frac{4}{3h^2} (\bar{P}_{yy,y}^{nl} + \bar{P}_{xy,x}^{nl}) ny + \bar{Q}'_{x}^{nl} n_x + \bar{Q}'_{y}^{nl} n_y + \\
& + (\bar{N}_{xx}^{nl} w_{0,x} + \bar{N}_{xy}^{nl} w_{0,y}) n_x + (\bar{N}_{yy}^{nl} w_{0,y} + \bar{N}_{xy}^{nl} w_{0,x}) n_y) \delta^2 w_0 - \frac{4}{3h^2} (\bar{P}_{xx}^{nl} nx + \\
& + \bar{P}_{xy}^{nl} ny) \delta^2 w_{0,x} - \frac{4}{3h^2} (\bar{P}_{yy}^{nl} ny + \bar{P}_{xy}^{nl} nx) \delta^2 w_{0,y}] + \\
& + [(\delta \bar{N}_{xx}^{nl} nx + \delta \bar{N}_{xy}^{nl} ny) \delta u_0 + (\delta \bar{N}_{xy}^{nl} nx + \delta \bar{N}_{yy}^{nl} ny) \delta v_0 + \\
& + \left(\left(\delta \bar{M}_{xx}^{nl} - \frac{4 \delta \bar{P}_{xx}^{nl}}{3h^2} \right) nx + \left(\delta \bar{M}_{xy}^{nl} - \frac{4 \delta \bar{P}_{xy}^{nl}}{3h^2} \right) ny \right) \delta \varphi_x + (\left(\delta \bar{M}_{yy}^{nl} - \frac{4 \delta \bar{P}_{yy}^{nl}}{3h^2} \right) ny + \\
& + \left(\delta \bar{M}_{xy}^{nl} - \frac{4 \delta \bar{P}_{xy}^{nl}}{3h^2} \right) nx) \delta \varphi_y + (\frac{4}{3h^2} (\delta \bar{P}_{xx,x}^{nl} + \delta \bar{P}_{xy,y}^{nl}) nx + \frac{4}{3h^2} (\delta \bar{P}_{yy,y}^{nl} + \delta \bar{P}_{xy,x}^{nl}) ny + \\
& + \delta \bar{Q}'_{x}^{nl} n_x + \delta \bar{Q}'_{y}^{nl} n_y + (\delta \bar{N}_{xx}^{nl} w_{0,x} + \delta \bar{N}_{xy}^{nl} w_{0,y}) n_x + (\delta \bar{N}_{yy}^{nl} w_{0,y} + \delta \bar{N}_{xy}^{nl} w_{0,x}) n_y) \delta w_0 - \\
& - \frac{4}{3h^2} (\delta \bar{P}_{xx}^{nl} nx + \delta \bar{P}_{xy}^{nl} ny) \delta w_{0,x} - \frac{4}{3h^2} (\delta \bar{P}_{yy}^{nl} ny + \delta \bar{P}_{xy}^{nl} nx) \delta w_{0,y}] \} ds
\end{aligned}$$

Substituting $\delta \Pi = 0$ (Hamilton's principle) and initially perfectly flat plates conditions ($w_{0,x} = w_{0,y} = 0$), Eq. (43) turns into:

$$\begin{aligned}
& \delta^2 \Pi = \int_{\Omega} \int_{-\frac{h}{2}}^{\frac{h}{2}} \{ [\bar{N}_{xx}^{nl} \delta w_{0,x}^2 + 2 \bar{N}_{xy}^{nl} \delta w_{0,x} \delta w_{0,y} + \bar{N}_{yy}^{nl} \delta w_{0,y}^2] + \\
& + [(-\delta \bar{N}_{xx,x}^{nl} - \delta \bar{N}_{xy,y}^{nl}) \delta u_0 + (-\delta \bar{N}_{yy,y}^{nl} - \delta \bar{N}_{xy,x}^{nl}) \delta v_0 + (-\delta \bar{M}_{xx,x}^{nl} - \delta \bar{M}_{xy,y}^{nl} + \\
& + \frac{4}{3h^2} (\delta \bar{P}_{xx,x}^{nl} + \delta \bar{P}_{xy,y}^{nl}) + \delta \bar{Q}'_{x}^{nl}) \delta \varphi_x + (-\delta \bar{M}_{yy,y}^{nl} - \delta \bar{M}_{xy,x}^{nl} + \frac{4}{3h^2} (\delta \bar{P}_{yy,y}^{nl} + \\
& + \delta \bar{P}_{xy,x}^{nl}) + \delta \bar{Q}'_{y}^{nl}) \delta \varphi_y + (-\frac{4}{3h^2} (\delta \bar{P}_{xx,xx}^{nl} + \delta \bar{P}_{yy,yy}^{nl} + 2 \delta \bar{P}_{xy,xy}^{nl}) - \\
& - K_p \nabla^2 \delta w_0 + K_w \delta w_0 - \delta \bar{Q}'_{x,x}^{nl} - \delta \bar{Q}'_{y,y}^{nl}) \delta w_0] \} dx \, dy + \\
& + \oint_{\Gamma} \{ [(\delta \bar{N}_{xx}^{nl} nx + \delta \bar{N}_{xy}^{nl} ny) \delta u_0 + (\delta \bar{N}_{xy}^{nl} nx + \delta \bar{N}_{yy}^{nl} ny) \delta v_0 +
\end{aligned} \tag{44}$$

$$\begin{aligned}
 & + \left(\left(\delta \bar{M}_{xx}^{nl} - \frac{4\delta \bar{P}_{xx}^{nl}}{3h^2} \right) nx + \left(\delta \bar{M}_{xy}^{nl} - \frac{4\delta \bar{P}_{xy}^{nl}}{3h^2} \right) ny \right) \delta \varphi_x + \left(\left(\delta \bar{M}_{yy}^{nl} - \frac{4\delta \bar{P}_{yy}^{nl}}{3h^2} \right) ny + \right. \\
 & \left. + \left(\delta \bar{M}_{xy}^{nl} - \frac{4\delta \bar{P}_{xy}^{nl}}{3h^2} \right) nx \right) \delta \varphi_y + \left(\frac{4}{3h^2} (\delta \bar{P}_{xx,x}^{nl} + \delta \bar{P}_{xy,y}^{nl}) nx + \right. \\
 & \left. + \frac{4}{3h^2} (\delta \bar{P}_{yy,y}^{nl} + \delta \bar{P}_{xy,x}^{nl}) ny + \delta \bar{Q}'_x^{nl} n_x + \delta \bar{Q}'_y^{nl} n_y \right) \delta w_0 - \\
 & - \frac{4}{3h^2} (\delta \bar{P}_{xx}^{nl} nx + \delta \bar{P}_{xy}^{nl} ny) \delta w_{0,x} - \frac{4}{3h^2} (\delta \bar{P}_{yy}^{nl} ny + \delta \bar{P}_{xy}^{nl} nx) \delta w_{0,y} \} ds
 \end{aligned}$$

We also can write:

$$\begin{aligned}
 & \int_{\Omega} \int_{-\frac{h}{2}}^{\frac{h}{2}} [\bar{N}_{xx}^{nl} \delta w_{0,x}^2 + 2 \bar{N}_{xy}^{nl} \delta w_{0,x} \delta w_{0,y} + \bar{N}_{yy}^{nl} \delta w_{0,y}^2] dx dy = \\
 & - \int_{\Omega} \int_{-\frac{h}{2}}^{\frac{h}{2}} [(\bar{N}_{xx}^{nl} \delta w_{0,x} + \bar{N}_{xy}^{nl} \delta w_{0,y})_{,x} + (\bar{N}_{yy}^{nl} \delta w_{0,y} + \bar{N}_{xy}^{nl} \delta w_{0,x})_{,y}] \delta w_0 dx dy + \\
 & + \oint_{\Gamma} ((\bar{N}_{xx}^{nl} \delta w_{0,x} + \bar{N}_{xy}^{nl} \delta w_{0,y}) nx + (\bar{N}_{yy}^{nl} \delta w_{0,y} + \bar{N}_{xy}^{nl} \delta w_{0,x}) ny) \delta w_0 ds
 \end{aligned} \quad (45)$$

From Eqs. (41), (44) and (45) the governing buckling equations are:

$$\delta u_0: \quad \delta \bar{N}_{xx,x} + \delta \bar{N}_{xy,y} = 0 \quad (46.1)$$

$$\delta v_0: \quad \delta \bar{N}_{yy,y} + \delta \bar{N}_{xy,x} = 0 \quad (46.2)$$

$$\delta \varphi_x: \quad -\delta \bar{M}_{xx,x} - \delta \bar{M}_{xy,y} + \frac{4}{3h^2} (\delta \bar{P}_{xx,x} + \delta \bar{P}_{xy,y}) + \delta \bar{Q}'_x = 0 \quad (46.3)$$

$$\delta \varphi_y: \quad -\delta \bar{M}_{yy,y} - \delta \bar{M}_{xy,x} + \frac{4}{3h^2} (\delta \bar{P}_{yy,y} + \delta \bar{P}_{xy,x}) + \delta \bar{Q}'_y = 0 \quad (46.4)$$

$$\begin{aligned}
 \delta w_0: \quad & -\frac{4}{3h^2} (\delta \bar{P}_{xx,xx} + \delta \bar{P}_{yy,yy} + 2 \delta \bar{P}_{xy,xy}) - K_p \mathbf{L} \nabla^2 \delta w_0 + K_w \mathbf{L} \delta w_0 - \delta \bar{Q}'_{x,x} - \\
 & - \delta \bar{Q}'_{y,y} + \bar{N}_{xx} \delta w_{0,xx} + 2 \bar{N}_{xy} \delta w_{0,xy} + \bar{N}_{yy} \delta w_{0,yy} = 0
 \end{aligned} \quad (46.5)$$

It can be shown that boundary condition can be written as (Reddy J. N. 2006):

$$\delta u_{0n} = 0 \quad \text{or} \quad \delta \bar{N}_{nn} = 0 \quad (47.1)$$

$$\delta u_{0s} = 0 \quad \text{or} \quad \delta \bar{N}_{ns} = 0 \quad (47.2)$$

$$\delta w_0 = 0 \quad \text{or} \quad \delta \bar{V}'_n = 0 \quad (47.3)$$

$$\delta \varphi_n = 0 \quad \text{or} \quad \delta \bar{M}_{nn} - \frac{4}{3h^2} \delta \bar{P}_{nn} = 0 \quad (47.4)$$

$$\delta\varphi_s = 0 \quad \text{or} \quad \delta\bar{M}_{ns} - \frac{4}{3h^2}\delta\bar{P}_{ns} = 0 \quad (47.5)$$

$$\frac{\partial\delta w_0}{\partial n} = 0 \quad \text{or} \quad \delta\bar{P}_{nn} = 0 \quad (47.6)$$

where

$$\begin{aligned} \delta\bar{V}'_n &= \left[\frac{4}{3h^2} (\delta\bar{P}_{xx,x}^{nl} + \delta\bar{P}_{xy,y}^{nl}) + \delta\bar{Q}'_x^{nl} + (\bar{N}_{xx}^{nl} \delta w_{0,x} + \bar{N}_{xy}^{nl} \delta w_{0,y}) \right] nx + \\ &+ \left[\frac{4}{3h^2} (\delta\bar{P}_{yy,y}^{nl} + \delta\bar{P}_{xy,x}^{nl}) + \delta\bar{Q}'_y^{nl} + (\bar{N}_{yy}^{nl} \delta w_{0,y} + \bar{N}_{xy}^{nl} \delta w_{0,x}) \right] ny \end{aligned} \quad (48)$$

Since the boundary conditions are homogenous we use following change of variables to solve linear Eqs. (46.1)-(46.5):

$$\begin{Bmatrix} \delta u_0(x, y, t) \\ \delta v_0(x, y, t) \\ \delta w_0(x, y, t) \\ \delta\varphi_x(x, y, t) \\ \delta\varphi_y(x, y, t) \end{Bmatrix} = \begin{Bmatrix} \delta U_0(x, y) \\ \delta V_0(x, y) \\ \delta W_0(x, y) \\ \delta\Phi_x(x, y) \\ \delta\Phi_y(x, y) \end{Bmatrix} e^{j\omega t} \quad (49)$$

It can be seen from Eqs. (46.1)-(46.5) that governing equations for buckling and vibration analysis are analogous, however in buckling equations we deal with the variations of resultant stresses and displacement. For biaxial compression loading (in the present research) we change the sign of \bar{N}_{xx} and \bar{N}_{yy} to minus and set:

$$\bar{N}_{xy} = 0 \quad \bar{N}_{yy} = \gamma\bar{N}_{xx} = \gamma N_{cr} \quad \gamma = 1 \quad (50)$$

5. Results and discussion

The numerical results presented in this section are devoted to illustrate the natural frequency and buckling responses of FG nano-plates under three cases of boundary conditions, including SSSS, CCCC, CSCS as:

a) SSSS (all edges are under movable simply-supported boundary condition):

$$\begin{aligned} V_0 &= W_0 = \Phi_Y = \hat{N}_{XX} = \hat{M}_{XX} = \hat{P}_{XX} = 0 && \text{at edge } s X = 0, 1 \\ U_0 &= W_0 = \Phi_X = \hat{N}_{YY} = \hat{M}_{YY} = \hat{P}_{YY} = 0 && \text{at edges } Y = 0, 1 \end{aligned} \quad (51)$$

b) CCCC (all edges are under clamped boundary conditions):

$$\begin{aligned} U_0 &= V_0 = W_0 = \Phi_X = \Phi_Y = \frac{\partial W_0}{\partial X} = 0 && \text{at edges } X = 0, 1 \\ U_0 &= V_0 = W_0 = \Phi_X = \Phi_Y = \frac{\partial W_0}{\partial Y} = 0 && \text{at edges } Y = 0, 1 \end{aligned} \quad (52)$$

c) CSCS (Two opposite edges are under clamped boundary conditions and the other edges are under movable simply-supported boundary conditions):

$$\begin{aligned} U_0 &= V_0 = W_0 = \Phi_X = \Phi_Y = \frac{\partial W_0}{\partial X} = 0 && \text{at edges } X = 0, 1 \\ U_0 &= W_0 = \Phi_X = \hat{N}_{YY} = \hat{M}_{YY} = \hat{P}_{YY} = 0 && \text{at edges } Y = 0, 1 \end{aligned} \quad (53)$$

Table 1 Temperature dependent material properties

Property	Material	P_{-1}	P_0	P_1	P_2	P_3	criteria
$E(Gpa)$	$Al^{1,3}$	0	82.1091	-4.4838E-04	5.8961E-08	-2.4700E-10	$0 \leq T(K) \leq 900$
	Si^2	0	127.5	-4.9412E-05	-3.4510E-08	0	
ν	Al^3	0	0.35				
	Si^6	0	0.24				
$\rho(Kg/m^3)$	$Al^{1,3}$	0	2727.2075	-3.2641E-05	1.6233E-08	-6.1935E-11	$0 \leq T(K) \leq 922$
	Si (Hull 1999)	0.2845103E4	$-0.1690T - 0.1750 - 3(T - 0.1687E4)^2$				
$\alpha (10^{-6}/K)$	$Al^{1,4}$	0	-2.1855	-7.0705E-02	1.2740E-04	-7.9704E-08	$25 \leq T \leq 900$
	Si (Hull 1999)			$0.3725E - 5 - 0.3725E$			
$\kappa(W/m K)$	$Al^{1,4}$	0	203.1537	1.0696E-03	-1.8995E-06	8.3775E-10	$0 \leq T \leq 933.52$
	Si^1 (Hull 1999)	0	412.0898	-2.5104E-03	2.1914E-06	-6.1993E-10	$200 \leq T \leq 1681$
$\tau_0(N/m)$	Al^4	0	1.0098	-1.5052E-04	-	-	
	Si (Hull 1999)	0	1.2461	-1.7655E-04	-	-	
$\lambda_0(N/m)$	Al^5	0	6.842	0	0	0	
	Si^5	0	-4.488	0	0	0	
$\mu_0(N/m)$	Al^5	0	-0.376	0	0	0	
	Si^5	0	-2.774	0	0	0	
$\rho_0(kg/m^2)$	Al^6	0	5.46E-7	0	0	0	
	Si^6	0	3.17E-7	0	0	0	

¹ The material property is obtained by the use of curve fitting method

² (Swarnakar, Biest, and Vanhellemont 2014)

³ (Mondolfo 2013)

⁴ (Aluminum Association 1984)

⁵ (Shaat, Mahmoud, Alshorbagy and Alieldin 2013)

⁶ (Ansari, Ashrafi, Pourashraf and Sahmani 2015)

the terms used in Eqs. (51)-(53) are defined in Eqs. (30) and (40).

The FG nano-plate studied in this section has the ceramic (silicon) at the top surface of the plate ($z = \frac{h}{2}$) and the metal (Al) at the bottom($z = -\frac{h}{2}$). It is supposed that material distribution changes as power-law (Eq. (12.1)) function continuously in the thickness direction of the nano-plate. The FG nano-plate is subjected to a thermal loading process where the bottom plane is held at $T_m = T_0 = 300 K$ ($\Delta T_m = 0$), while the temperature of the upper plane of the plate is risen

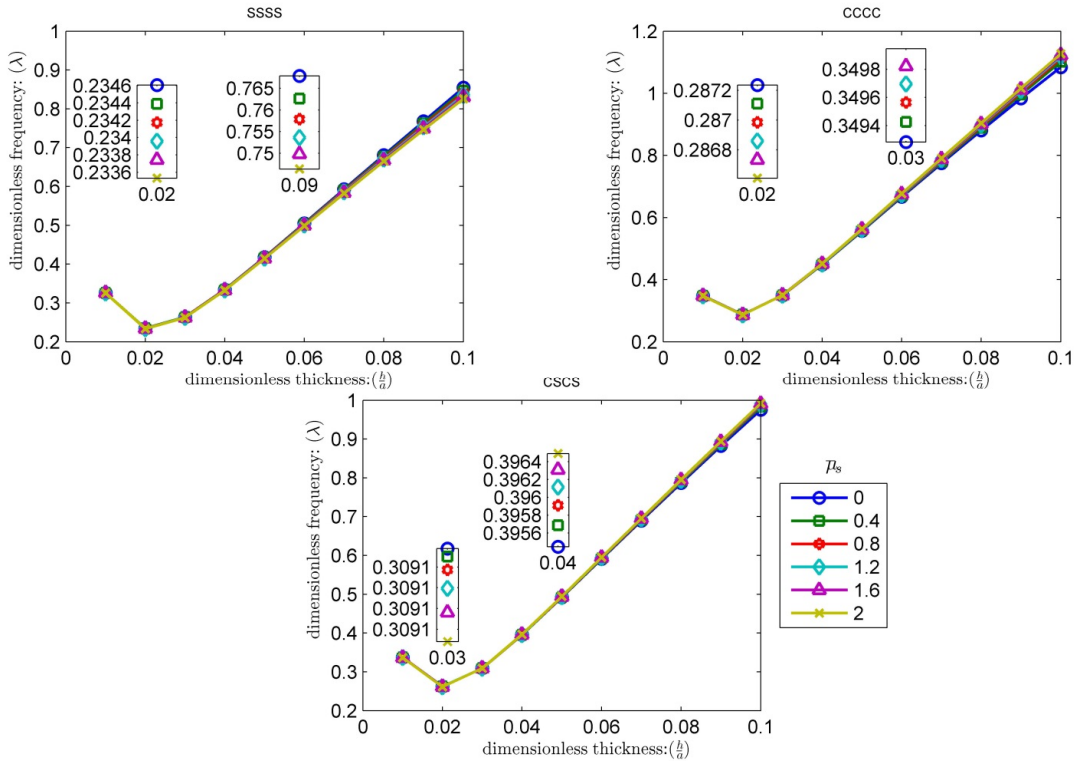


Fig. 2 Influence of nonlocal parameter on dimensionless fundamental natural frequencies of square (Al/Si) FG Reddy nano-plate with respect to various dimensionless thickness for different boundary conditions, considering surface stresses effect ($\bar{K}_w = 100, \bar{K}_p = 30, p = 3, a = 200 nm, \Delta T_c = 450 K, \Delta C = C_c = 0, \Delta E_0 = 1$)

from $T_0 = 300 K$ to $T_0 + \Delta T_c$ (unless otherwise specified, the temperature rise for upper plane of the plate is $\Delta T_c = 450 K$); the midpoints experience the nonlinear temperature rise as illustrated in Eq. (23). Under temperature lower than boiling point, the effect of moisture concentration will be studied in this section where the moisture concentration and temperature are risen simultaneously; it is assumed the moisture absorption is elated to ceramic and is linear as explained in Eq. (24).

The results are gained using DQ (Shu 2012) and iterative method (Ebrahimi and Hosseini 2016a, Malekzadeh 2007). To study dimensionless frequency ($\lambda = \omega a \sqrt{\frac{\rho_c(T_0, h/2)}{E_c(T_0, h/2)}}$) and dimensionless buckling load ($\bar{N}_{cr} = \frac{N_{cr} h}{E_c(T_0, h/2) a^2}$) the material properties are taken into consideration as given in Table 1.

Fig. 2 shows the dimensionless frequency variation versus dimensionless thickness considering nonlocal parameter's variation in thermal environment; beyond the absolute minimum point (at around $\frac{h}{a} = 0.02$), dimensionless thickness rising has increasing effect on dimensionless frequency, however the influence of nonlocal parameter on frequency is dependent to boundary condition status; for full simply supported boundary condition rising nonlocal parameter decreases

the dimensionless frequency but for other boundary condition there is an intersect point; before the intersect point rising of nonlocal parameter decreases the frequency however after the intersect point the effect is vice versa. To show the effect of nonlocal parameter on dimensionless critical buckling load (Fig. 3) we set the dimensionless elastic foundation as:

$$\bar{K}_W = 100, \bar{K}_p = 30 \quad (54)$$

where

$$\bar{K}_W = \frac{K_W a^4}{D_c} \quad \bar{K}_p = \frac{K_p a^2}{D_c} \quad D_c = \frac{E_c \left(\frac{h}{2}, T_0 \right) h^3}{12 (1 - v_c \left(\frac{h}{2}, T_0 \right))^2} \quad (55)$$

From Fig. 3 one can conclude that rising the nonlocal parameter and dimensionless thickness increases buckling load and in the result the plate will be more stable. The numerical results for these figures and for hyperbolic shear deformation plate theory are available in Table 2. A comparison study between different boundary condition shows that values that are related to CCCC boundary condition are higher than other boundary condition while SSSS boundary condition appropriates minimum values.

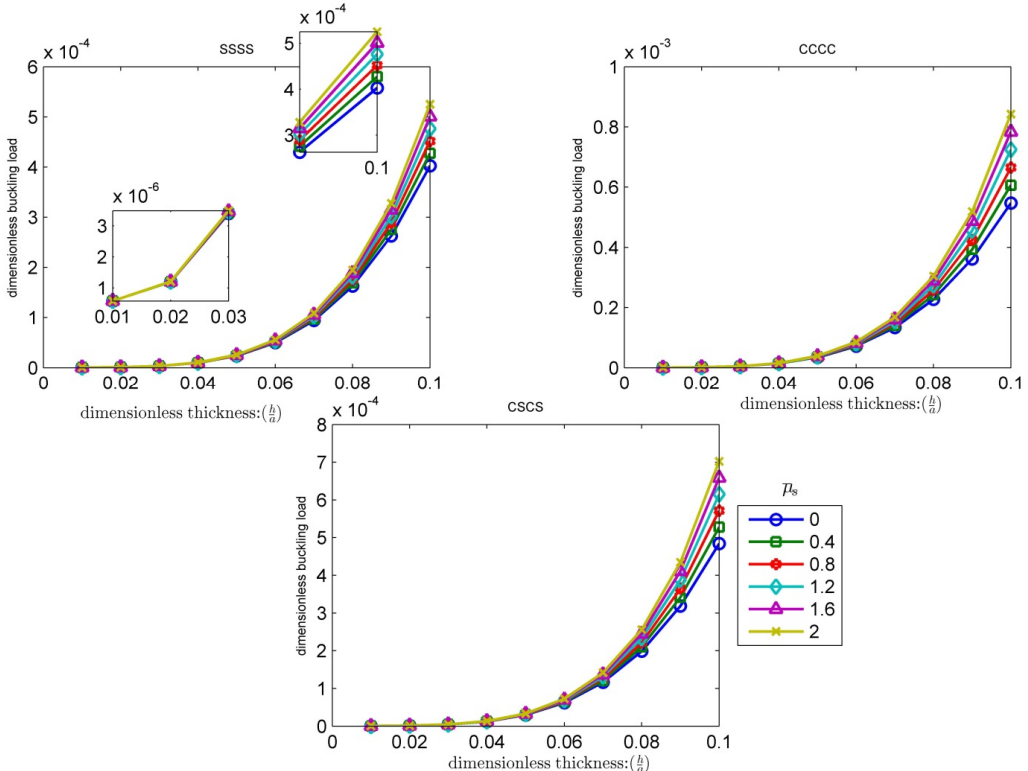


Fig. 3 Influence of nonlocal parameter on dimensionless critical buckling load of square (Al/Si) FG Reddy nano-plate with respect to various dimensionless thickness for different boundary conditions, considering surface stresses effect ($\bar{K}_w = 100, \bar{K}_p = 30, p = 3, a = 200 \text{ nm}, \Delta T_c = 450 \text{ K}, \Delta C = C_c = 0, \Delta E_0 = 1$)

Table 2 Influence of nonlocal parameter on dimensionless fundamental natural frequency and dimensionless critical buckling load of (*Al/Si*) FG Reddy and Hyperbolic shear deformation square nano-plate with respect to various dimensionless thickness for different boundary conditions, considering surface stresses effect ($\bar{K}_w = 100$, $\bar{K}_p = 30$, $p = 3$, $a = 200 \text{ nm}$, $\Delta T_c = 450 \text{ K}$, $\Delta C = C_c = 0$, $\Delta E_0 = 1$)

$\bar{\mu}$	h/a	SSSS			CCCC			CSCS			
		λ_{nl}	λ_{nl}/λ_l	\bar{N}_σ	λ_{nl}	λ_{nl}/λ_l	\bar{N}_σ	λ_{nl}	λ_{nl}/λ_l	\bar{N}_σ	
0	0.01	RPT	0.3261	1.0002	5.7940E-07	0.3479	1.0003	5.9699E-07	0.3372	1.0002	5.8917E-07
		HSDPT	0.3261	1.0002	5.7940E-07	0.3479	1.0003	5.9699E-07	0.3372	1.0002	5.8917E-07
	0.05	RPT	0.4178	1.0014	2.3811E-05	0.5573	1.0028	3.4671E-05	0.4922	1.0020	2.9877E-05
		HSDPT	0.4177	1.0014	2.3811E-05	0.5567	1.0026	3.4672E-05	0.4919	1.0019	2.9877E-05
	0.1	RPT	0.8545	1.0012	4.0280E-04	1.0838	1.0023	5.4684E-04	0.9757	1.0016	4.8406E-04
		HSDPT	0.8511	1.0010	4.0280E-04	1.0724	1.0010	5.4685E-04	0.9686	1.0009	4.8407E-04
	0.4	RPT	0.3260	1.0002	5.7942E-07	0.3478	1.0003	5.9705E-07	0.3370	1.0002	5.8922E-07
		HSDPT	0.3260	1.0002	5.7942E-07	0.3478	1.0003	5.9705E-07	0.3370	1.0002	5.8922E-07
		RPT	0.4170	1.0014	2.4194E-05	0.5588	1.0027	3.5596E-05	0.4928	1.0019	3.0559E-05
		HSDPT	0.4169	1.0014	2.4194E-05	0.5581	1.0025	3.5596E-05	0.4925	1.0018	3.0559E-05
		RPT	0.8472	1.0011	4.2728E-04	1.1019	1.0022	6.0615E-04	0.9833	1.0016	5.2776E-04
		HSDPT	0.8438	1.0009	4.2728E-04	1.0888	1.0011	6.0615E-04	0.9755	1.0010	5.2776E-04
0.8	0.01	RPT	0.3258	1.0002	5.7945E-07	0.3477	1.0003	5.9711E-07	0.3369	1.0002	5.8926E-07
		HSDPT	0.3258	1.0002	5.7945E-07	0.3477	1.0003	5.9711E-07	0.3369	1.0002	5.8926E-07
	0.05	RPT	0.4163	1.0014	2.4576E-05	0.5600	1.0027	3.6521E-05	0.4933	1.0019	3.1241E-05
		HSDPT	0.4162	1.0014	2.4576E-05	0.5594	1.0025	3.6521E-05	0.4930	1.0018	3.1241E-05
	0.1	RPT	0.8409	1.0011	4.5176E-04	1.1117	1.0022	6.6531E-04	0.9868	1.0015	5.7142E-04
		HSDPT	0.8375	1.0009	4.5176E-04	1.0975	1.0011	6.6531E-04	0.9786	1.0009	5.7142E-04
	1.2	RPT	0.3257	1.0002	5.7947E-07	0.3476	1.0003	5.9717E-07	0.3368	1.0002	5.8930E-07
		HSDPT	0.3257	1.0002	5.7947E-07	0.3476	1.0003	5.9717E-07	0.3368	1.0002	5.8930E-07
		RPT	0.4156	1.0014	2.4959E-05	0.5611	1.0027	3.7445E-05	0.4938	1.0019	3.1923E-05
		HSDPT	0.4155	1.0014	2.4959E-05	0.5605	1.0025	3.7445E-05	0.4934	1.0018	3.1923E-05
		RPT	0.8353	1.0010	4.7625E-04	1.1184	1.0021	7.2443E-04	0.9891	1.0014	6.1507E-04
		HSDPT	0.8320	1.0008	4.7625E-04	1.1023	1.0000	7.2444E-04	0.9805	1.0009	6.1507E-04
1.6	0.01	RPT	0.3256	1.0002	5.7949E-07	0.3474	1.0003	5.9723E-07	0.3367	1.0002	5.8935E-07
		HSDPT	0.3256	1.0002	5.7949E-07	0.3474	1.0003	5.9723E-07	0.3367	1.0002	5.8935E-07
	0.05	RPT	0.4149	1.0014	2.5341E-05	0.5622	1.0026	3.8369E-05	0.4942	1.0018	3.2605E-05
		HSDPT	0.4148	1.0013	2.5341E-05	0.5615	1.0024	3.8369E-05	0.4938	1.0018	3.2605E-05
	0.1	RPT	0.8304	1.0010	5.0073E-04	1.1233	1.0020	7.8354E-04	0.9906	1.0014	6.5872E-04
		HSDPT	0.8262	0.9997	5.0073E-04	1.1068	1.0000	7.8355E-04	0.9818	1.0009	6.5872E-04

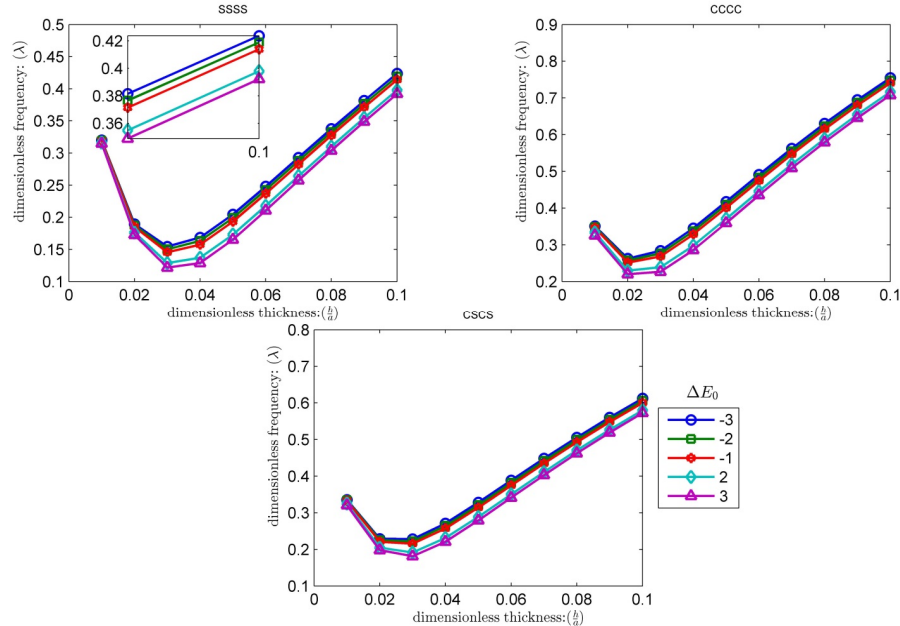


Fig. 4 Influence of surface elastic modulus differential on dimensionless fundamental natural frequencies of square (Al/Si) FG Reddy nano-plate with respect to various dimensionless thickness for different boundary conditions, considering surface stresses effect ($\bar{K}_w = \bar{K}_p = 0, p = 3, \bar{\mu} = 0.2, a = 200 nm, \Delta T_c = 450 K, \Delta C = C_c = 0$)

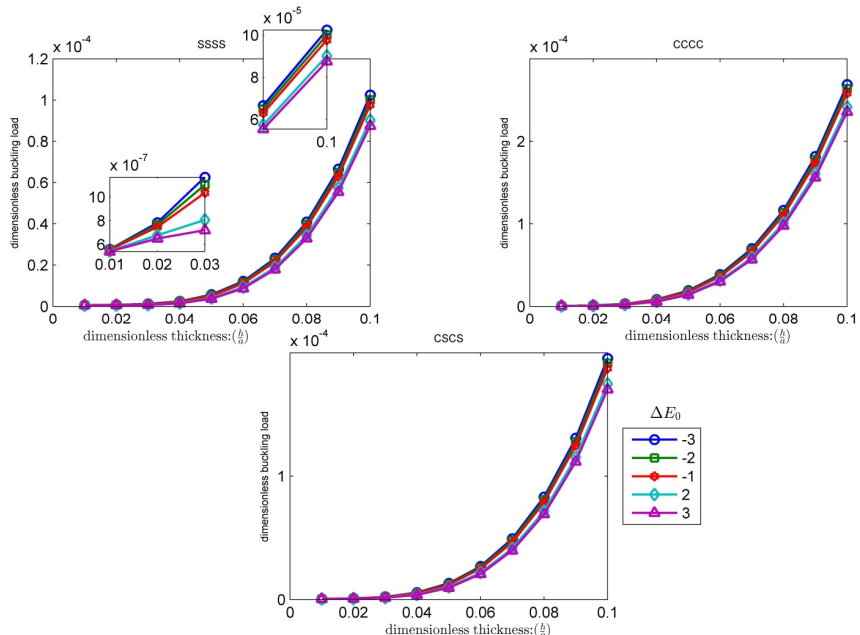


Fig. 5 Influence of surface elastic modulus differential on dimensionless critical buckling load of square (Al/Si) FG Reddy nano-plate with respect to various dimensionless thickness for different boundary conditions, considering surface stresses effect ($\bar{K}_w = \bar{K}_p = 0, p = 3, \bar{\mu} = 0.2, a = 200 nm, \Delta T_c = 450 K, \Delta C = C_c = 0$)

Table 3 Influence of surface elastic modulus differential on dimensionless fundamental natural frequency and dimensionless buckling load of (Al/Si) FG Reddy and Hyperbolic shear deformation square nano-plate with respect to various dimensionless thickness for different boundary conditions, considering surface stresses effect ($\bar{K}_w = \bar{K}_p = 0, p = 3, \bar{\mu} = 0.2, a = 200 nm, \Delta T_c = 450 K, \Delta C = C_c = 0$)

		SSSS			CCCC			CSCS			
ΔE_0^1	h/a	λ_{nl}	λ_{nl}/λ_l	\bar{N}_σ	λ_{nl}	λ_{nl}/λ_l	\bar{N}_σ	λ_{nl}	λ_{nl}/λ_l	\bar{N}_σ	
-3	0.01	RPT	0.3199	1.0001	5.5805E-07	0.3508	1.0003	5.9259E-07	0.3357	1.0002	5.7719E-07
		HSDPT	0.3199	1.0001	5.5805E-07	0.3508	1.0003	5.9259E-07	0.3357	1.0002	5.7719E-07
	0.05	RPT	0.2046	1.0049	5.7281E-06	0.4175	1.0052	1.9203E-05	0.3282	1.0042	1.3226E-05
		HSDPT	0.2045	1.0048	5.7281E-06	0.4169	1.0048	1.9203E-05	0.3279	1.0040	1.3226E-05
	0.1	RPT	0.4238	1.0039	1.0246E-04	0.7548	1.0050	2.6877E-04	0.6124	1.0039	1.9542E-04
		HSDPT	0.4216	1.0029	1.0246E-04	0.7444	1.0022	2.6877E-04	0.6066	1.0022	1.9542E-04
	-2	RPT	0.3194	1.0001	5.5617E-07	0.3487	1.0003	5.8763E-07	0.3343	1.0002	5.7360E-07
		HSDPT	0.3194	1.0001	5.5617E-07	0.3487	1.0003	5.8763E-07	0.3343	1.0002	5.7360E-07
		RPT	0.1992	1.0054	5.4216E-06	0.4093	1.0055	1.8436E-05	0.3213	1.0045	1.2662E-05
		HSDPT	0.1991	1.0053	5.4216E-06	0.4087	1.0051	1.8436E-05	0.3210	1.0043	1.2662E-05
		RPT	0.4190	1.0041	1.0010E-04	0.7476	1.0051	2.6358E-04	0.6063	1.0040	1.9147E-04
		HSDPT	0.4168	1.0031	1.0010E-04	0.7374	1.0023	2.6358E-04	0.6006	1.0023	1.9147E-04
	-1	RPT	0.3188	1.0001	5.5400E-07	0.3462	1.0003	5.8188E-07	0.3327	1.0002	5.6944E-07
		HSDPT	0.3188	1.0001	5.5400E-07	0.3462	1.0003	5.8188E-07	0.3327	1.0002	5.6944E-07
		RPT	0.1934	1.0060	5.1037E-06	0.4006	1.0059	1.7639E-05	0.3139	1.0049	1.2077E-05
		HSDPT	0.1933	1.0059	5.1037E-06	0.4000	1.0054	1.7639E-05	0.3137	1.0046	1.2077E-05
		RPT	0.4140	1.0043	9.7691E-05	0.7403	1.0053	2.5826E-04	0.6000	1.0041	1.8743E-04
		HSDPT	0.4119	1.0033	9.7692E-05	0.7302	1.0024	2.5826E-04	0.5945	1.0024	1.8743E-04
2	0.01	RPT	0.3161	1.0001	5.4469E-07	0.3339	1.0003	5.5726E-07	0.3251	1.0002	5.5166E-07
		HSDPT	0.3161	1.0001	5.4469E-07	0.3339	1.0003	5.5726E-07	0.3251	1.0002	5.5166E-07
		RPT	0.1732	1.0086	4.0749E-06	0.3708	1.0073	1.5051E-05	0.2887	1.0063	1.0179E-05
		HSDPT	0.1731	1.0084	4.0749E-06	0.3704	1.0068	1.5051E-05	0.2885	1.0060	1.0179E-05
		RPT	0.3980	1.0049	9.0157E-05	0.7166	1.0057	2.4154E-04	0.5798	1.0046	1.7476E-04
		HSDPT	0.3960	1.0038	9.0158E-05	0.7070	1.0027	2.4154E-04	0.5746	1.0028	1.7476E-04
	0.05	RPT	0.3148	1.0002	5.4012E-07	0.3257	1.0003	5.4515E-07	0.3203	1.0002	5.4291E-07
		HSDPT	0.3148	1.0002	5.4012E-07	0.3257	1.0003	5.4515E-07	0.3203	1.0002	5.4291E-07
		RPT	0.1654	1.0099	3.7044E-06	0.3595	1.0079	1.4115E-05	0.2791	1.0069	9.4933E-06
		HSDPT	0.1653	1.0097	3.7044E-06	0.3590	1.0074	1.4115E-05	0.2789	1.0067	9.4934E-06
		RPT	0.3923	1.0051	8.7539E-05	0.7081	1.0059	2.3569E-04	0.5726	1.0048	1.7033E-04
		HSDPT	0.3903	1.0040	8.7540E-05	0.6987	1.0029	2.3570E-04	0.5675	1.0029	1.7034E-04

$$\Delta E_0 = \frac{E_0^+ - E_0^-}{E_{01}^+ - E_{01}^-}$$

In Fig. 4 and Fig. 5, influence of the surface elastic modulus differential ($\Delta E_0 = \frac{E_0^+ - E_0^-}{E_{01}^+ - E_{01}^-}$, $E_0 = 2\mu_0 + \lambda_0$) on the dimensionless fundamental frequency and the dimensionless critical buckling load of FG nano-plate is investigated (the surface residual stress (τ_0) is considered temperature dependent). The frequency and buckling load are plotted versus dimensionless thickness when the surface elastic modulus differential varies. Like the previous case for dimensionless thickness variation the dimensionless frequency has an absolute minimum value whereupon the results increase by increasing the dimensionless thickness; however the dimensionless buckling load strictly increases by rising dimensionless thickness. It is observed that by increasing ΔE_0 the dimensionless frequency and buckling load reduce however during increasing of dimensionless thickness the constant elastic modulus differential curves ($\Delta E_0 = \text{const}$) converge with each other; this means by increasing the dimensionless thickness the effect of surface will be weakened. The corresponding results are listed in Table 3; the numerical results for hyperbolic shear deformation plate theory are also available in this table.

Fig. 6 and Fig. 7 depict the effect of the volume fraction exponent on the natural frequency and critical buckling load of FG nano-plate, respectively. It is clear that with increasing in volume fraction exponent value the frequency and buckling load decreases. Under CCCC boundary condition the related values are higher than other boundary condition. Table 4 presents the related results which can be compared with the results of hyperbolic shear deformation plate theory.

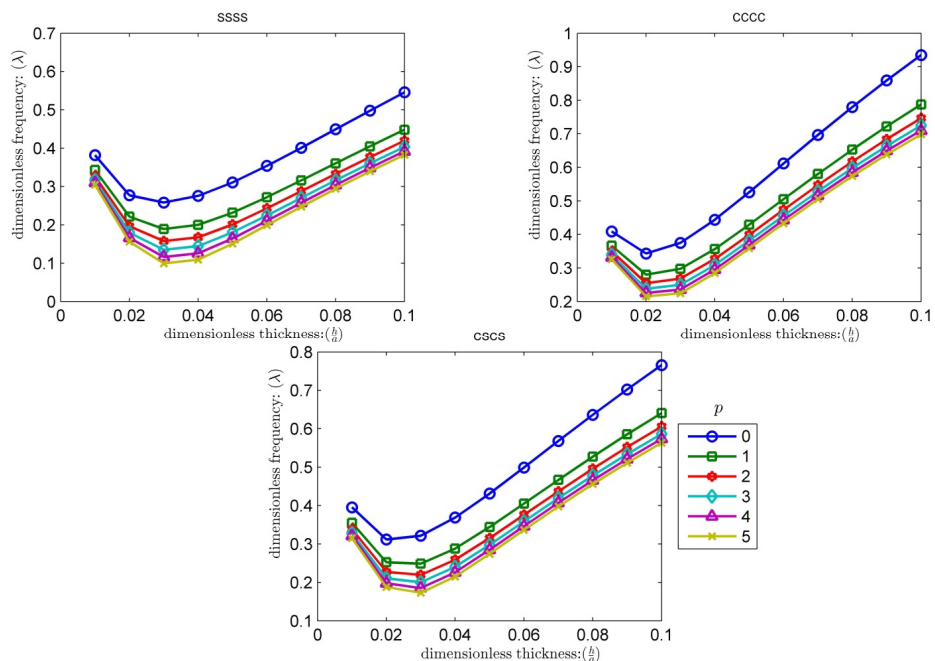


Fig. 6. Influence of volume fraction exponent on dimensionless fundamental natural frequencies of square (Al/Si) FG Reddy nano-plate with respect to various dimensionless thickness for different boundary conditions, considering surface stresses effect ($\bar{K}_w = \bar{K}_p = 0$, $\bar{\mu} = 0.2$, $a = 200$ nm, $\Delta T_c = 450$ K, $\Delta C = C_c = 0$, $\Delta E_0 = 1$)

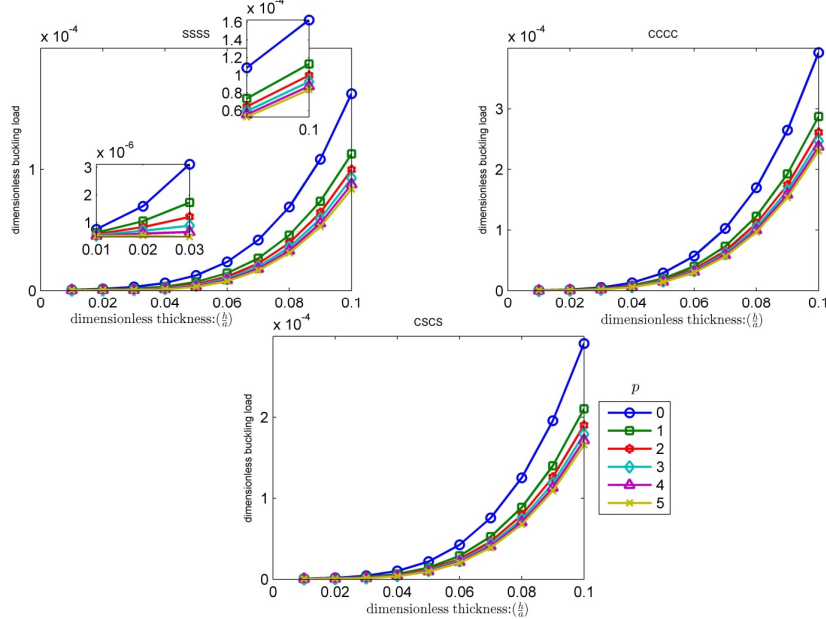


Fig. 7. Influence of volume fraction exponent on dimensionless critical buckling load of square (Al/Si) FG Reddy nano-plate with respect to various dimensionless thickness for different boundary conditions, considering surface stresses effect ($\bar{K}_w = \bar{K}_p = 0, \bar{\mu} = 0.2, a = 200 nm, \Delta T_c = 450 K, \Delta C = C_c = 0, \Delta E_0 = 1$)

Table 4 Influence of volume fraction exponent on dimensionless fundamental natural frequency and dimensionless critical buckling load of (Al/Si) FG Reddy and Hyperbolic shear deformation square nano-plate with respect to various dimensionless thickness for different boundary conditions, considering surface stresses effect ($\bar{K}_w = \bar{K}_p = 0, \bar{\mu} = 0.2, a = 200 nm, \Delta T_c = 450 K, \Delta C = C_c = 0, \Delta E_0 = 1$)

p	h/a	SSSS				CCCC				CSCS			
		λ_{nl}	λ_{nl}/λ_l	\bar{N}_{σ}									
0	0.01	RPT	0.3819	1.0001	7.5678E-07	0.4088	1.0002	7.8325E-07	0.3955	1.0002	7.7144E-07		
		HSDPT	0.3819	1.0001	7.5678E-07	0.4088	1.0002	7.8325E-07	0.3955	1.0002	7.7144E-07		
	0.05	RPT	0.3107	1.0022	1.2637E-05	0.5259	1.0037	2.9211E-05	0.4313	1.0027	2.1849E-05		
		HSDPT	0.3106	1.0021	1.2637E-05	0.5254	1.0035	2.9211E-05	0.4311	1.0026	2.1849E-05		
	0.1	RPT	0.5460	1.0019	1.6253E-04	0.9348	1.0036	3.9271E-04	0.7659	1.0025	2.9110E-04		
		HSDPT	0.5440	1.0015	1.6253E-04	0.9246	1.0016	3.9271E-04	0.7603	1.0014	2.9110E-04		
	1	RPT	0.3432	1.0002	6.3239E-07	0.3665	1.0003	6.5309E-07	0.3550	1.0002	6.4386E-07		
		HSDPT	0.3432	1.0002	6.3239E-07	0.3665	1.0003	6.5309E-07	0.3550	1.0002	6.4386E-07		
	0.05	RPT	0.2317	1.0055	7.2256E-06	0.4292	1.0062	1.9966E-05	0.3442	1.0051	1.4308E-05		
		HSDPT	0.2316	1.0054	7.2256E-06	0.4287	1.0058	1.9966E-05	0.3440	1.0049	1.4308E-05		
	0.1	RPT	0.4482	1.0046	1.1277E-04	0.7876	1.0056	2.8733E-04	0.6410	1.0045	2.1029E-04		
		HSDPT	0.4462	1.0037	1.1277E-04	0.7779	1.0029	2.8733E-04	0.6357	1.0028	2.1029E-04		

Table 4 (continued)

2	0.01	RPT	0.3272	1.0002	5.8104E-07	0.3497	1.0003	6.0043E-07	0.3386	1.0002	5.9178E-07
		HSDPT	0.3272	1.0002	5.8104E-07	0.3497	1.0003	6.0043E-07	0.3386	1.0002	5.9178E-07
0.05	RPT	0.2009	1.0067	5.4766E-06	0.3990	1.0066	1.7401E-05	0.3153	1.0055	1.2108E-05	
		HSDPT	0.2008	1.0065	5.4766E-06	0.3985	1.0062	1.7401E-05	0.3150	1.0053	1.2108E-05
0.1	RPT	0.4196	1.0048	9.9822E-05	0.7466	1.0057	2.6103E-04	0.6059	1.0046	1.8991E-04	
		HSDPT	0.4176	1.0037	9.9823E-05	0.7369	1.0028	2.6103E-04	0.6005	1.0028	1.8991E-04
4	0.01	RPT	0.3099	1.0002	5.2496E-07	0.3315	1.0003	5.4305E-07	0.3209	1.0002	5.3498E-07
		HSDPT	0.3099	1.0002	5.2496E-07	0.3315	1.0003	5.4305E-07	0.3209	1.0002	5.3498E-07
0.05	RPT	0.1644	1.0084	3.6809E-06	0.3686	1.0068	1.4912E-05	0.2847	1.0059	9.9281E-06	
		HSDPT	0.1643	1.0083	3.6810E-06	0.3681	1.0063	1.4912E-05	0.2845	1.0056	9.9281E-06
0.1	RPT	0.3919	1.0045	8.7699E-05	0.7099	1.0054	2.3782E-04	0.5736	1.0043	1.7160E-04	
		HSDPT	0.3899	1.0035	8.7700E-05	0.7002	1.0025	2.3783E-04	0.5683	1.0025	1.7161E-04
5	0.01	RPT	0.3044	1.0002	5.0708E-07	0.3257	1.0003	5.2470E-07	0.3152	1.0002	5.1684E-07
		HSDPT	0.3044	1.0002	5.0708E-07	0.3257	1.0003	5.2470E-07	0.3152	1.0002	5.1684E-07
0.05	RPT	0.1509	1.0094	3.0999E-06	0.3584	1.0069	1.4103E-05	0.2743	1.0060	9.2205E-06	
		HSDPT	0.1508	1.0092	3.0999E-06	0.3579	1.0064	1.4103E-05	0.2740	1.0057	9.2206E-06
0.1	RPT	0.3827	1.0044	8.3784E-05	0.6986	1.0053	2.3065E-04	0.5635	1.0042	1.6587E-04	
		HSDPT	0.3808	1.0034	8.3785E-05	0.6890	1.0024	2.3066E-04	0.5582	1.0024	1.6587E-04

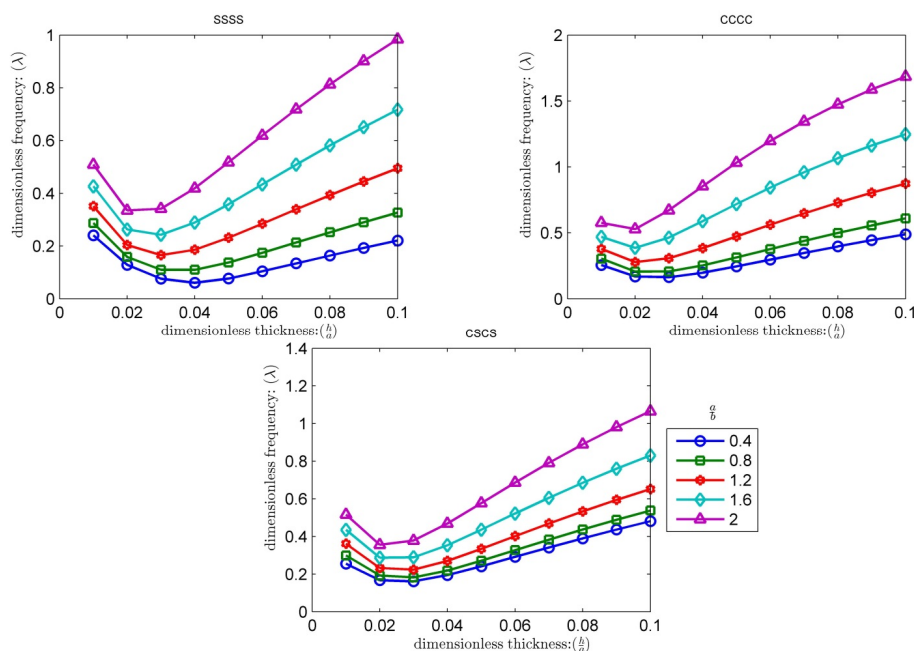


Fig. 8. Influence of aspect ratio on dimensionless fundamental natural frequencies of (Al/Si) FG Reddy nano-plate with respect to various dimensionless thickness for different boundary conditions, considering surface stresses effect ($\bar{K}_w = \bar{K}_p = 0, p = 3, \bar{\mu} = 0.2, a = 200 nm, \Delta T_c = 450 K, \Delta C = C_c = 0, \Delta E_0 = 0$)

Fig. 8 and Fig. 9 demonstrate the influence of aspect ratio on the natural frequency and critical buckling load of the FG nano-plate in thermal environment and under different boundary conditions; it can also be seen with the increase in aspect ratio the natural frequency and critical buckling load will enhance. For SSSS boundary condition the effect of aspect ratio is more sensible than other boundary condition whereas the higher values are related to CCCC boundary condition. The numerical results for this case and hyperbolic shear deformation plate theory are available in Table 5.

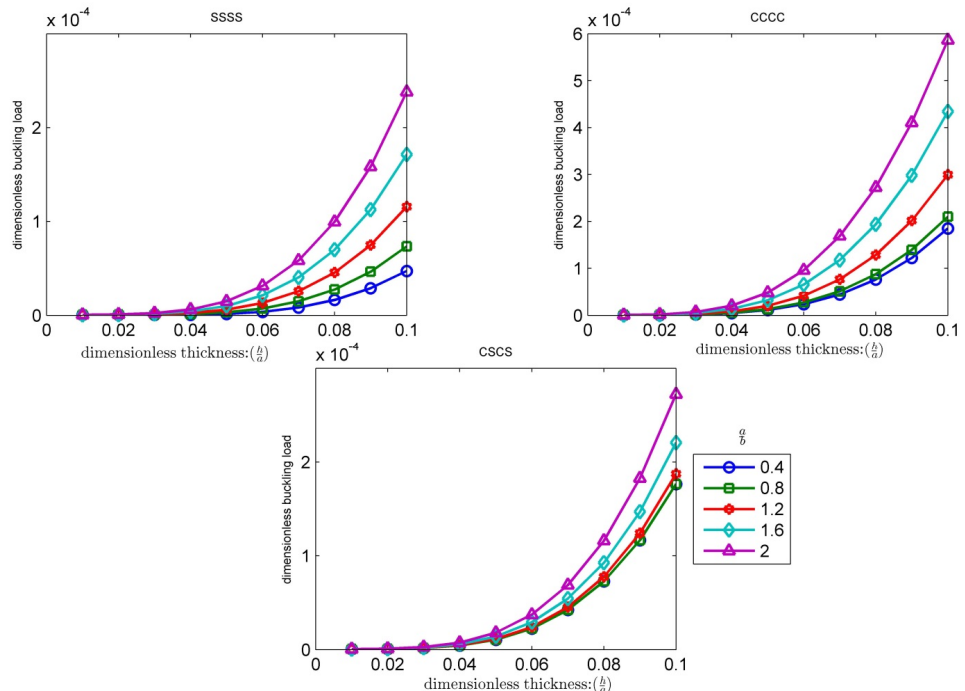


Fig. 9 Influence of aspect ratio on dimensionless critical buckling load of (Al/Si) FG Reddy nano-plate with respect to various dimensionless thickness for different boundary conditions, considering surface stresses effect ($\bar{K}_w = \bar{K}_p = 0, p = 3, \bar{\mu} = 0.2, a = 200 \text{ nm}, \Delta T_c = 450 \text{ K}, \Delta C = C_c = 0, \Delta E_0 = 1$)

Table 5 Influence of aspect ratio on dimensionless fundamental natural frequency and dimensionless critical buckling load of (Al/Si) FG Reddy and hyperbolic shear deformation nano-plate with respect to various dimensionless thickness for different boundary conditions, considering surface stresses effect ($\bar{K}_w = \bar{K}_p = 0, p = 3, \bar{\mu} = 0.2, a = 200 \text{ nm}, \Delta T_c = 450 \text{ K}, \Delta C = C_c = 0, \Delta E_0 = 0$)

a/b	h/a	SSSS			CCCC			CSCS			
		λ_{nl}	λ_{nl}/λ_l	\bar{N}_{σ}	λ_{nl}	λ_{nl}/λ_l	\bar{N}_{σ}	λ_{nl}	λ_{nl}/λ_l	\bar{N}_{σ}	
0.4	0.01	RPT	0.2405	1.0001	5.4364E-07	0.2558	1.0001	5.5909E-07	0.2549	1.0001	5.5832E-07
		HSDPT	0.2405	1.0001	5.4364E-07	0.2558	1.0001	5.5909E-07	0.2549	1.0001	5.5832E-07
0.05	RPT	0.0767	1.0056	1.3773E-06	0.2457	1.0056	1.1125E-05	0.2412	1.0046	1.0608E-05	
		HSDPT	0.0767	1.0055	1.3773E-06	0.2455	1.0054	1.1125E-05	0.2411	1.0044	1.0608E-05
0.1	RPT	0.2210	1.0022	4.7177E-05	0.4889	1.0047	1.8518E-04	0.4810	1.0039	1.7663E-04	

Table 5 (continued)

		HSDPT	0.2207	1.0020	4.7177E-05	0.4856	1.0029	1.8518E-04	0.4779	1.0024	1.7663E-04
0.8	0.01	RPT	0.2867	1.0001	5.4635E-07	0.3049	1.0002	5.6227E-07	0.2989	1.0002	5.5832E-07
		HSDPT	0.2867	1.0001	5.4635E-07	0.3049	1.0002	5.6227E-07	0.2989	1.0002	5.5832E-07
	0.05	RPT	0.1375	1.0083	3.1274E-06	0.3136	1.0068	1.3055E-05	0.2711	1.0055	1.0608E-05
		HSDPT	0.1375	1.0082	3.1274E-06	0.3133	1.0065	1.3056E-05	0.2709	1.0053	1.0608E-05
	0.1	RPT	0.3268	1.0046	7.3490E-05	0.6099	1.0055	2.1023E-04	0.5376	1.0044	1.7663E-04
		HSDPT	0.3256	1.0038	7.3491E-05	0.6037	1.0031	2.1024E-04	0.5334	1.0027	1.7663E-04
1.2	0.01	RPT	0.3511	1.0002	5.5088E-07	0.3785	1.0004	5.7423E-07	0.3613	1.0002	5.5978E-07
		HSDPT	0.3511	1.0002	5.5088E-07	0.3785	1.0004	5.7423E-07	0.3613	1.0002	5.5978E-07
	0.05	RPT	0.2316	1.0064	6.0144E-06	0.4729	1.0063	2.0227E-05	0.3338	1.0056	1.1477E-05
		HSDPT	0.2315	1.0062	6.0145E-06	0.4720	1.0057	2.0228E-05	0.3335	1.0053	1.1478E-05
	0.1	RPT	0.4948	1.0042	1.1566E-04	0.8737	1.0054	2.9945E-04	0.6520	1.0043	1.8736E-04
		HSDPT	0.4914	1.0030	1.1566E-04	0.8580	1.0021	2.9945E-04	0.6450	1.0024	1.8736E-04
1.6	0.01	RPT	0.4265	1.0002	5.5721E-07	0.4701	1.0005	5.9557E-07	0.4349	1.0003	5.6391E-07
		HSDPT	0.4265	1.0002	5.5721E-07	0.4701	1.0005	5.9557E-07	0.4349	1.0003	5.6391E-07
	0.05	RPT	0.3585	1.0043	9.9952E-06	0.7185	1.0055	3.2434E-05	0.4359	1.0047	1.4003E-05
		HSDPT	0.3581	1.0041	9.9953E-06	0.7157	1.0043	3.2434E-05	0.4352	1.0044	1.4003E-05
	0.1	RPT	0.7170	1.0031	1.7140E-04	1.2481	1.0053	4.3453E-04	0.8304	1.0036	2.2070E-04
		HSDPT	0.7082	1.0018	1.7140E-04	1.2096	1.0012	4.3454E-04	0.8173	1.0018	2.2070E-04
2	0.01	RPT	0.5090	1.0003	5.6534E-07	0.5763	1.0007	6.2544E-07	0.5162	1.0003	5.7054E-07
		HSDPT	0.5090	1.0003	5.6534E-07	0.5763	1.0007	6.2544E-07	0.5162	1.0003	5.7054E-07
	0.05	RPT	0.5175	1.0029	1.5011E-05	1.0327	1.0049	4.8414E-05	0.5770	1.0036	1.8028E-05
		HSDPT	0.5165	1.0026	1.5011E-05	1.0251	1.0030	4.8415E-05	0.5756	1.0032	1.8028E-05
	0.1	RPT	0.9840	1.0023	2.3796E-04	1.6851	1.0054	5.8671E-04	1.0657	1.0028	2.7231E-04
		HSDPT	0.9639	1.0011	2.3797E-04	1.6031	1.0000	5.8672E-04	1.0409	1.0012	2.7232E-04

Dimensionless fundamental frequency and dimensionless critical buckling load variations of the FG nano-plate is presented in Fig. 10 and Fig. 11 for various values of elastic foundation parameters and dimensionless thickness in thermal environment and under different boundary conditions. At first glance, it can be found that by changing Winkler modulus for a constant shear modulus there is miserly variation for fundamental frequency and critical buckling load which imply unimportant effect of Winkler parameter on frequency and critical buckling load than shear modulus; however, when the value of shear modulus has increasing variation, this results in the growth of the frequency and the critical buckling load. The numerical results for this case and hyperbolic shear deformation plate theory have been listed it tables Table 6.

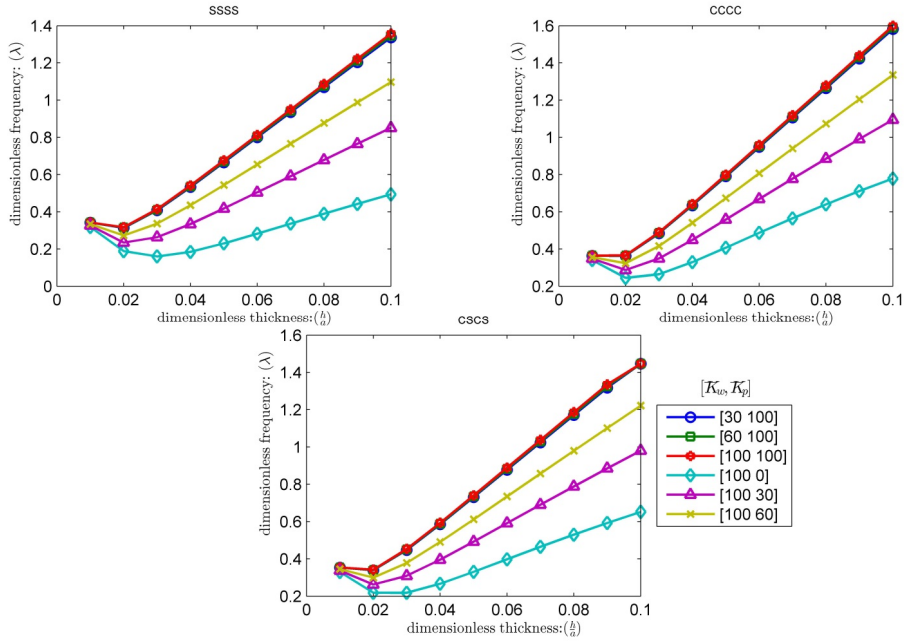


Fig. 10 Influence of Pasternak and Winkler parameters on dimensionless fundamental natural frequencies of square (Al/Si) FG Reddy nano-plate with respect to various dimensionless thickness for different boundary conditions, considering surface stresses effect ($p = 3, \bar{\mu} = 0.2, a = 200 \text{ nm}, \Delta T_c = 450 \text{ K}, \Delta C = C_c = 0, \Delta E_0 = 1$)

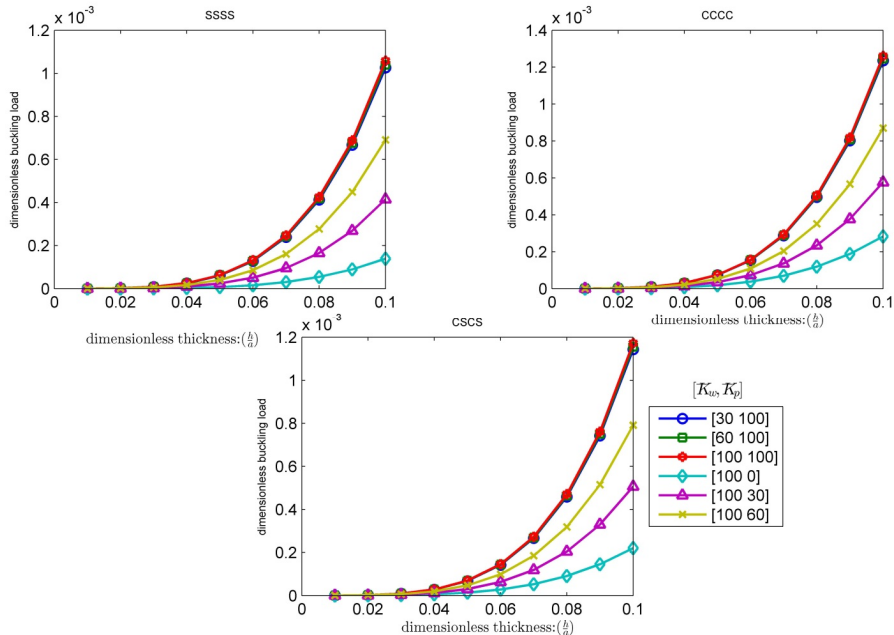


Fig. 11. Influence of Pasternak and Winkler parameters on dimensionless critical buckling load of square (Al/Si) FG Reddy nano-plate with respect to various dimensionless thickness for different boundary conditions, considering surface stresses effect ($p = 3, \bar{\mu} = 0.2, a = 200 \text{ nm}, \Delta T_c = 450 \text{ K}, \Delta C = C_c = 0, \Delta E_0 = 1$)

Table 6 Influence of Pasternak and Winkler parameters on dimensionless fundamental natural frequency and dimensionless critical buckling load of (Al/Si) FG Reddy and hyperbolic shear deformation square nanoplate with respect to various dimensionless thickness for different boundary conditions, considering surface stresses effect ($p = 3, \bar{\mu} = 0.2, a = 200 nm, \Delta T_c = 450 K, \Delta C = C_c = 0, \Delta E_0 = 1$)

\bar{K}_w	\bar{K}_p	h/a	SSSS			CCCC			CSCS		
			λ_{nl}	λ_{nl}/λ_l	\bar{N}_{σ}	λ_{nl}	λ_{nl}/λ_l	\bar{N}_{σ}	λ_{nl}	λ_{nl}/λ_l	\bar{N}_{σ}
100	0	0.01	RPT	0.3185	1.0002 5.5287E-07	0.3403	1.0003 5.7047E-07	0.3296	1.0002 5.6265E-07		
			HSDPT	0.3185	1.0002 5.5287E-07	0.3403	1.0003 5.7047E-07	0.3296	1.0002 5.6265E-07		
		0.05	RPT	0.2303	1.0046 7.2586E-06	0.4074	1.0059 1.8119E-05	0.3303	1.0047 1.3324E-05		
			HSDPT	0.2302	1.0045 7.2586E-06	0.4069	1.0055 1.8119E-05	0.3300	1.0045 1.3324E-05		
		0.1	RPT	0.4938	1.0032 1.3929E-04	0.7787	1.0048 2.8333E-04	0.6522	1.0036 2.2055E-04		
			HSDPT	0.4915	1.0025 1.3929E-04	0.7685	1.0023 2.8334E-04	0.6465	1.0022 2.2056E-04		
	30	0.01	RPT	0.3260	1.0002 5.7941E-07	0.3479	1.0003 5.9702E-07	0.3371	1.0002 5.8919E-07		
			HSDPT	0.3260	1.0002 5.7941E-07	0.3479	1.0003 5.9702E-07	0.3371	1.0002 5.8919E-07		
		0.05	RPT	0.4174	1.0014 2.4002E-05	0.5581	1.0028 3.5134E-05	0.4926	1.0019 3.0218E-05		
			HSDPT	0.4173	1.0014 2.4002E-05	0.5575	1.0026 3.5134E-05	0.4922	1.0019 3.0218E-05		
		0.1	RPT	0.8507	1.0012 4.1504E-04	1.0950	1.0023 5.7654E-04	0.9805	1.0016 5.0592E-04		
			HSDPT	0.8473	1.0009 4.1504E-04	1.0825	1.0011 5.7654E-04	0.9731	1.0010 5.0593E-04		
100	60	0.01	RPT	0.3334	1.0002 6.0595E-07	0.3552	1.0003 6.2358E-07	0.3445	1.0002 6.1574E-07		
			HSDPT	0.3334	1.0002 6.0595E-07	0.3552	1.0003 6.2358E-07	0.3445	1.0002 6.1574E-07		
		0.05	RPT	0.5436	1.0009 4.0746E-05	0.6731	1.0018 5.2149E-05	0.6117	1.0012 4.7111E-05		
			HSDPT	0.5434	1.0008 4.0746E-05	0.6724	1.0016 5.2149E-05	0.6113	1.0011 4.7111E-05		
		0.1	RPT	1.0971	1.0008 6.9079E-04	1.3355	1.0015 8.6966E-04	1.2222	1.0010 7.9127E-04		
			HSDPT	1.0930	1.0006 6.9079E-04	1.3213	1.0007 8.6966E-04	1.2134	1.0006 7.9127E-04		
	100	0.01	RPT	0.3430	1.0002 6.4133E-07	0.3647	1.0003 6.5899E-07	0.3540	1.0002 6.5114E-07		
			HSDPT	0.3430	1.0002 6.4133E-07	0.3647	1.0003 6.5899E-07	0.3540	1.0002 6.5114E-07		
		0.05	RPT	0.6761	1.0006 6.3071E-05	0.7992	1.0012 7.4835E-05	0.7401	1.0008 6.9636E-05		
			HSDPT	0.6759	1.0006 6.3071E-05	0.7983	1.0011 7.4835E-05	0.7396	1.0008 6.9636E-05		
		0.1	RPT	1.3577	1.0006 1.0585E-03	1.5997	1.0011 1.2605E-03	1.4464	1.0000 1.1717E-03		
			HSDPT	1.3531	1.0005 1.0585E-03	1.5835	1.0005 1.2605E-03	1.4466	1.0000 1.1717E-03		

Fig. 12 and Fig. 13 illustrate the variation of the dimensionless fundamental natural frequency and dimensionless critical buckling load of square FG nano-plates versus the dimensionless thickness for different value of temperature rise of the upper plane of the plate. From these figures it can be observed that dimensionless fundamental frequency and critical buckling load decrease by the increase in aforesaid temperature; we can also conclude that temperature variation effect on natural frequency and critical buckling load is more sensible under SSSS boundary condition than other boundary conditions, because of the large distance between curves. The numerical results for this figures and hyperbolic shear deformation plate theory are tabulated in Table 7.

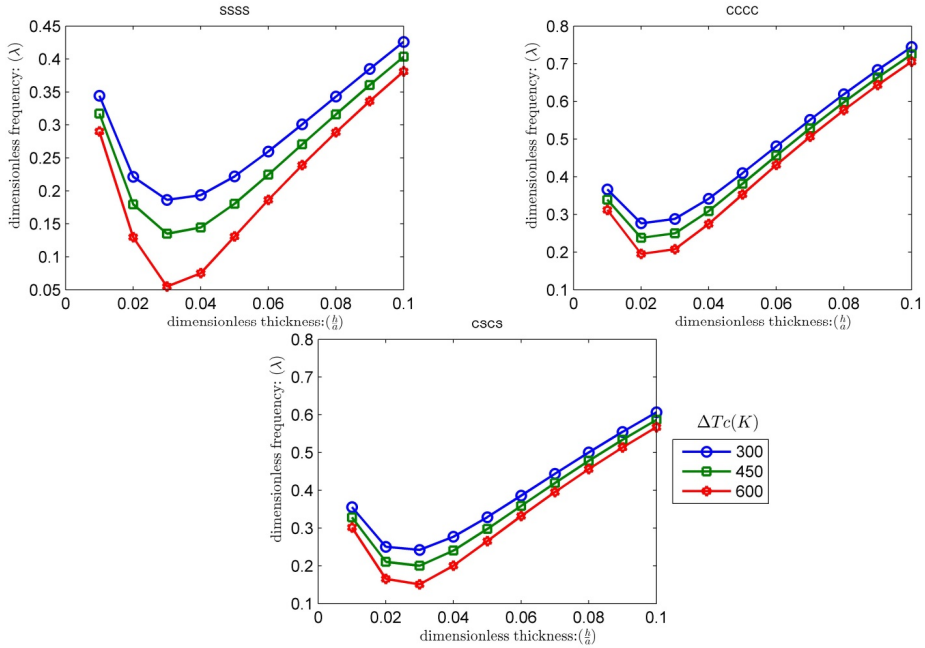


Fig. 12 Influence of thermal loading on dimensionless fundamental natural frequencies of square (Al/Si) FG Reddy nano-plate with respect to various dimensionless thickness for different boundary conditions, considering surface stresses effect ($\bar{K}_w = \bar{K}_p = 0, p = 3, \bar{\mu} = 0.2, a = 200 nm, \Delta C = C_c = 0, \Delta E_0 = 1$)

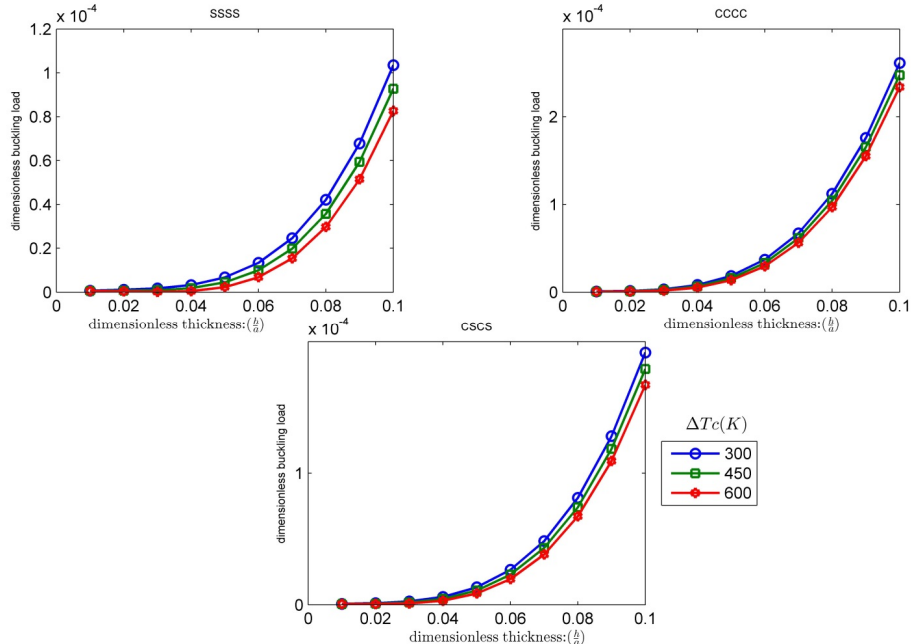


Fig. 13 Influence of thermal loading on dimensionless critical buckling load of square (Al/Si) FG Reddy nano-plate with respect to various dimensionless thickness for different boundary conditions, considering surface stresses effect ($\bar{K}_w = \bar{K}_p = 0, p = 3, \bar{\mu} = 0.2, a = 200 nm, \Delta C = C_c = 0, \Delta E_0 = 1$)

Table 7 Influence of thermal loading on dimensionless fundamental natural frequency and dimensionless critical buckling load of (*Al/Si*) FG Reddy and hyperbolic shear deformation square nano-plate with respect to various dimensionless thickness for different boundary conditions, considering surface stresses effect ($\bar{K}_w = \bar{K}_p = 0, p = 3, \bar{\mu} = 0.2, a = 200\text{ nm}, \Delta C = C_c = 0, \Delta E_0 = 1$)

$\Delta T_c(K)$	h/a		SSSS			CCCC			CSCS		
			λ_{nl}	λ_{nl}/λ_l	\bar{N}_{cr}	λ_{nl}	λ_{nl}/λ_l	\bar{N}_{cr}	λ_{nl}	λ_{nl}/λ_l	\bar{N}_{cr}
300	0.01	RPT	0.3442	1.0002	6.4592E-07	0.3662	1.0003	6.6501E-07	0.3554	1.0002	6.5649E-07
		HSDPT	0.3442	1.0002	6.4592E-07	0.3662	1.0003	6.6501E-07	0.3554	1.0002	6.5649E-07
		RPT	0.2220	1.0051	6.7433E-06	0.4095	1.0058	1.8492E-05	0.3288	1.0047	1.3278E-05
		HSDPT	0.2220	1.0050	6.7433E-06	0.4090	1.0054	1.8492E-05	0.3286	1.0045	1.3278E-05
		RPT	0.4261	1.0043	1.0348E-04	0.7444	1.0054	2.6129E-04	0.6068	1.0042	1.9168E-04
		HSDPT	0.4240	1.0033	1.0348E-04	0.7346	1.0025	2.6130E-04	0.6013	1.0025	1.9168E-04
	0.05	RPT	0.3172	1.0002	5.4839E-07	0.3391	1.0003	5.6704E-07	0.3283	1.0002	5.5872E-07
		HSDPT	0.3172	1.0002	5.4839E-07	0.3391	1.0003	5.6704E-07	0.3283	1.0002	5.5872E-07
		RPT	0.1804	1.0076	4.4311E-06	0.3814	1.0067	1.5949E-05	0.2977	1.0057	1.0837E-05
		HSDPT	0.1804	1.0074	4.4311E-06	0.3809	1.0063	1.5949E-05	0.2975	1.0055	1.0837E-05
		RPT	0.4035	1.0047	9.2720E-05	0.7248	1.0056	2.4724E-04	0.5868	1.0044	1.7908E-04
		HSDPT	0.4015	1.0036	9.2721E-05	0.7150	1.0026	2.4725E-04	0.5815	1.0026	1.7908E-04
450	0.01	RPT	0.2901	1.0002	4.5833E-07	0.3119	1.0004	4.7652E-07	0.3012	1.0003	4.6841E-07
		HSDPT	0.2901	1.0002	4.5833E-07	0.3119	1.0004	4.7652E-07	0.3012	1.0003	4.6841E-07
		RPT	0.1309	1.0143	2.2992E-06	0.3531	1.0079	1.3576E-05	0.2655	1.0072	8.5713E-06
		HSDPT	0.1308	1.0140	2.2992E-06	0.3527	1.0073	1.3576E-05	0.2653	1.0069	8.5714E-06
		RPT	0.3812	1.0051	8.2618E-05	0.7055	1.0058	2.3377E-04	0.5673	1.0046	1.6709E-04
		HSDPT	0.3792	1.0039	8.2618E-05	0.6959	1.0027	2.3378E-04	0.5620	1.0028	1.6710E-04
	0.05	RPT	0.2901	1.0002	4.5833E-07	0.3119	1.0004	4.7652E-07	0.3012	1.0003	4.6841E-07
		HSDPT	0.2901	1.0002	4.5833E-07	0.3119	1.0004	4.7652E-07	0.3012	1.0003	4.6841E-07
		RPT	0.1309	1.0143	2.2992E-06	0.3531	1.0079	1.3576E-05	0.2655	1.0072	8.5713E-06
		HSDPT	0.1308	1.0140	2.2992E-06	0.3527	1.0073	1.3576E-05	0.2653	1.0069	8.5714E-06
		RPT	0.3812	1.0051	8.2618E-05	0.7055	1.0058	2.3377E-04	0.5673	1.0046	1.6709E-04
		HSDPT	0.3792	1.0039	8.2618E-05	0.6959	1.0027	2.3378E-04	0.5620	1.0028	1.6710E-04

The influence of moisture concentration variation on dimensionless fundamental frequency and dimensionless critical buckling load can be seen in Fig. 14 and Fig. 15. Similar to thermal loading, moisture concentration variation has a contrary effect on the frequency and critical buckling load, meaning an increase in moisture concentration decreases the fundamental frequency and critical buckling load, however compared with temperature variation, moisture concentration has lower effect on the frequency and critical buckling load variation. The numerical results can be found and compared with the results of hyperbolic shear deformation plate theory in Table 8.

To verify the solution for critical buckling load a comparison study has been done with the results published in Ref. (Reddy, Kumar, Reddy and Reddy 2013) in Table 9; this article consider a third order shear deformation *Al/Al₂O₃* FG rectangular plate. Setting surface, nonlocal and elastic parameters to zero and neglecting the effect of temperature and moisture concentration and considering $\frac{a}{b} = 0.5$ it can be seen that there is a good agreement between the present buckling load and those of aforesaid reference. The material properties for this study are considered as:

$$\begin{aligned} E_m &= 70\text{ GPa}, \rho_m = 2702\text{ kg/m}^3, v = 0.3 && \text{For Aluminum} \\ E_c &= 380\text{ GPa}, \rho_c = 3800\text{ kg/m}^3, v = 0.3 && \text{For Alumina} \end{aligned} \quad (56)$$

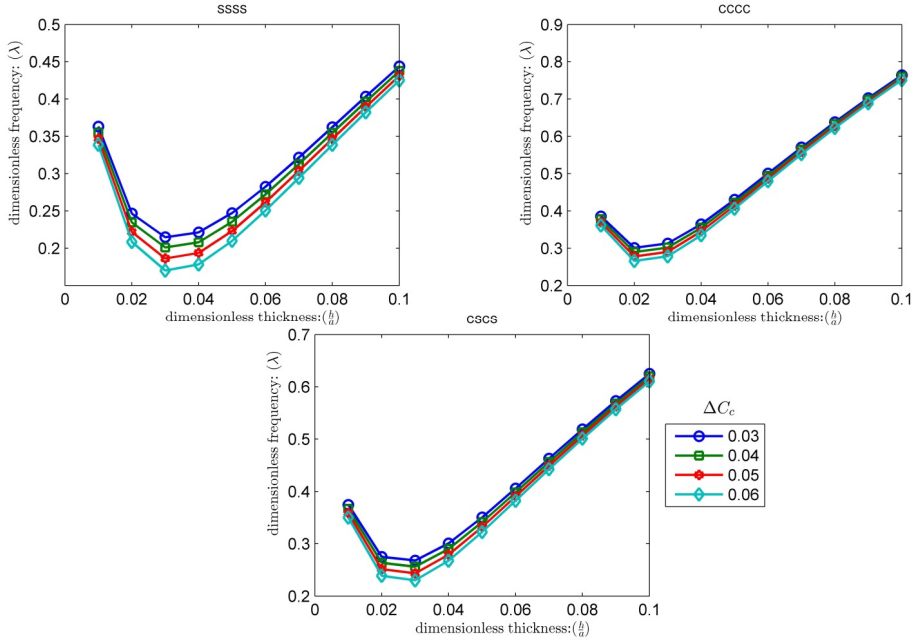


Fig. 14 Influence of moisture concentration variation on dimensionless fundamental natural frequencies of square (Al/Si) FG Reddy nano-plate with respect to various dimensionless thickness for different boundary conditions, considering surface stresses effect ($\bar{K}_w = \bar{K}_p = 0, p = 3, \bar{\mu} = 0.2, a = 200 nm, \Delta T_c = 70 K, \Delta E_0 = 1$)

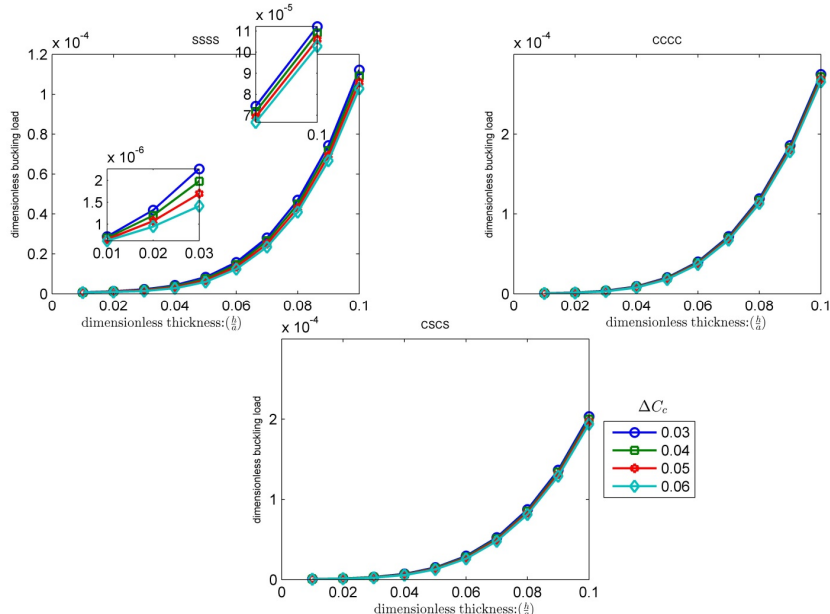


Fig. 15 Influence of moisture concentration variation on dimensionless critical buckling load of square (Al/Si) FG Reddy nano-plate with respect to various dimensionless thickness for different boundary conditions, considering surface stresses effect ($\bar{K}_w = \bar{K}_p = 0, p = 3, \bar{\mu} = 0.2, a = 200 nm, \Delta T_c = 70 K, \Delta E_0 = 1$)

Table 8 Influence of moisture concentration variation on dimensionless fundamental natural frequency and dimensionless critical buckling load of (*Al/Si*) FG Reddy and hyperbolic shear deformation square nanoplate with respect to various dimensionless thickness for different boundary conditions, considering surface stresses effect ($\bar{K}_w = \bar{K}_p = 0, p = 3, \bar{\mu} = 0.2, a = 200 \text{ nm}, \Delta T_c = 70 \text{ K}, \Delta E_0 = 1$)

$\Delta C_c = C_c$	h/a	SSSS			CCCC			CSCS				
		λ_{nl}	λ_{nl}/λ_l	\bar{N}_σ	λ_{nl}	λ_{nl}/λ_l	\bar{N}_σ	λ_{nl}	λ_{nl}/λ_l	\bar{N}_σ		
0.03	0.01	RPT	0.3633	1.0001	7.1872E-07	0.3856	1.0002	7.3844E-07	0.3746	1.0002	7.2964E-07	
		HSDPT	0.3633	1.0001	7.1872E-07	0.3856	1.0002	7.3844E-07	0.3746	1.0002	7.2964E-07	
	0.05	RPT	0.2472	1.0042	8.3628E-06	0.4303	1.0054	2.0456E-05	0.3504	1.0043	1.5088E-05	
		HSDPT	0.2471	1.0041	8.3628E-06	0.4298	1.0050	2.0456E-05	0.3501	1.0041	1.5088E-05	
	0.1	RPT	0.4439	1.0041	1.1221E-04	0.7639	1.0053	2.7500E-04	0.6249	1.0041	2.0318E-04	
		HSDPT	0.4417	1.0032	1.1221E-04	0.7539	1.0025	2.7500E-04	0.6195	1.0025	2.0319E-04	
	0.04	0.01	RPT	0.3553	1.0002	6.8730E-07	0.3777	1.0002	7.0702E-07	0.3666	1.0002	6.9823E-07
			HSDPT	0.3553	1.0002	6.8730E-07	0.3777	1.0002	7.0702E-07	0.3666	1.0002	6.9823E-07
		0.05	RPT	0.2354	1.0046	7.5774E-06	0.4223	1.0056	1.9670E-05	0.3413	1.0045	1.4303E-05
			HSDPT	0.2353	1.0045	7.5775E-06	0.4218	1.0052	1.9671E-05	0.3411	1.0043	1.4303E-05
		0.1	RPT	0.4377	1.0042	1.0907E-04	0.7597	1.0053	2.7186E-04	0.6202	1.0042	2.0004E-04
			HSDPT	0.4356	1.0033	1.0907E-04	0.7498	1.0026	2.7186E-04	0.6147	1.0025	2.0004E-04
	0.05	0.01	RPT	0.3470	1.0002	6.5589E-07	0.3695	1.0003	6.7561E-07	0.3584	1.0002	6.6681E-07
			HSDPT	0.3470	1.0002	6.5589E-07	0.3695	1.0003	6.7561E-07	0.3584	1.0002	6.6681E-07
		0.05	RPT	0.2230	1.0052	6.7921E-06	0.4142	1.0059	1.8885E-05	0.3320	1.0048	1.3518E-05
			HSDPT	0.2229	1.0051	6.7921E-06	0.4137	1.0055	1.8885E-05	0.3318	1.0046	1.3518E-05
		0.1	RPT	0.4314	1.0043	1.0593E-04	0.7556	1.0054	2.6872E-04	0.6154	1.0043	1.9690E-04
			HSDPT	0.4293	1.0034	1.0593E-04	0.7457	1.0026	2.6872E-04	0.6100	1.0026	1.9690E-04
	0.06	0.01	RPT	0.3386	1.0002	6.2447E-07	0.3611	1.0003	6.4419E-07	0.3501	1.0002	6.3540E-07
			HSDPT	0.3386	1.0002	6.2447E-07	0.3611	1.0003	6.4419E-07	0.3501	1.0002	6.3540E-07
		0.05	RPT	0.2098	1.0058	6.0067E-06	0.4059	1.0062	1.8100E-05	0.3225	1.0051	1.2732E-05
			HSDPT	0.2098	1.0057	6.0067E-06	0.4054	1.0058	1.8100E-05	0.3222	1.0049	1.2732E-05
		0.1	RPT	0.4250	1.0044	1.0279E-04	0.7514	1.0055	2.6557E-04	0.6106	1.0043	1.9376E-04
			HSDPT	0.4229	1.0035	1.0279E-04	0.7415	1.0026	2.6558E-04	0.6052	1.0026	1.9376E-04

6. Conclusions

In this work, the vibration and buckling behaviors of FG rectangular nano-plates subjected to hygro-thermal loading were investigated including the effect of surface stress. The governing equations were derived based on Reddy's plate theory, hyperbolic shear deformation plate theory and von Karman's nonlinearity assumption. DQ and iterative methods were applied to obtain solutions for fundamental frequency and critical buckling load. Knowing that obtained governing equations are dimensionless, to set logical values for dimensionless parameters the properties of Al/Si FGM were used. The numerical results show that:

- With the increase of dimensionless thickness ratio, before an absolute minimum value the

Table 9 Comparison of dimensionless critical buckling load ($\bar{N}_{cr} = \frac{N_{cr} a^2}{E_m h^3}$) of rectangular (Al/Al_2O_3) FG plate ($\bar{K}_w = \bar{K}_p = 0, \bar{\mu} = 0, a = 0.2m, \rho_{0m} = \rho_{0c} = 0, \lambda_{0m} = \mu_{0m} = \tau_{0m} = \lambda_{0c} = \mu_{0c} = \tau_{0c} = 0$). Material properties are according to Eq. (56)

a/b	h/a	source	Volume fraction exponent, p							
			0	0.5	1	2	5	10	20	100
0.5	0.2	present	5.3762	3.5392	2.7331	2.1161	1.7187	1.5370	1.3692	1.0989
		Ref (Reddy, Kumar, Reddy and Reddy 2013)	5.3710	3.5270	2.7150	2.0920	1.7000	1.5270	1.3640	1.0970
		Error (%)	0.0977	0.3453	0.6661	1.1516	1.1026	0.6566	0.3827	0.1748
0.5	0.1	present	5.9243	3.8569	2.9689	2.3117	1.9332	1.7517	1.5510	1.2200
		Ref (Reddy, Kumar, Reddy and Reddy 2013)	5.9180	3.8500	2.9610	2.3020	1.9250	1.7470	1.5480	1.2180
		Error (%)	0.1058	0.1803	0.2660	0.4226	0.4240	0.2679	0.1933	0.1644
0.5	0.05	present	6.0794	3.9456	3.0344	2.3665	1.9955	1.8152	1.6044	1.2546
		Ref (Reddy, Kumar, Reddy and Reddy 2013)	6.0720	3.9400	3.0290	2.3620	1.9910	1.8120	1.6020	1.2530
		Error (%)	0.1223	0.1430	0.1791	0.1916	0.2281	0.1767	0.1471	0.1300
0.5	0.02	present	6.1244	3.9712	3.0533	2.3823	2.0137	1.8338	1.6200	1.2647
		Ref (Reddy, Kumar, Reddy and Reddy 2013)	6.1170	3.9660	3.0490	2.3790	2.0110	1.8310	1.6180	1.2630
		Error (%)	0.1203	0.1314	0.1414	0.1406	0.1366	0.1547	0.1219	0.1334
0.5	0.01	present	6.1308	3.9749	3.0560	2.3846	2.0164	1.8365	1.6222	1.2661
		Ref (Reddy, Kumar, Reddy and Reddy 2013)	6.1230	3.9700	3.0520	2.3820	2.0140	1.8340	1.6200	1.2650
		Error (%)	0.1280	0.1233	0.1319	0.1101	0.1179	0.1377	0.1375	0.0897

frequency is decreasing however for higher value of the thickness ration with the increase of thickness ratio the fundamental frequency will increase. The critical buckling load will be enhanced when dimensionless thickness ration increases.

2. With the increase in nonlocal parameter, the dimensionless critical buckling load increases, however such effect on fundamental frequency is dependent on type of boundary condition and dimensionless thickness ratio; under simply supported boundary condition the increase in nonlocal parameter, the fundamental frequency decreases; under other boundary condition situation, when the thickness ratio is small enough, the increase of nonlocal parameter decreases the frequency but for larger value of thickness ratio this is vice versa.

3. Knowing that the residual surface stress (τ_0) is temperature dependent, the rising of the surface parameters, decreases the fundamental frequency and critical buckling load of FG nano-plate. It can be seen when the thickness ration increases the effect of surface parameters decreases.

4. The increase of volume fraction exponent decreases the fundamental frequency and critical buckling load of FG nano-plate.

5. With the increase in aspect ratio the natural frequency and critical buckling load will

enhance.

6. The effect of shear modulus of the elastic foundation on the fundamental natural frequency and critical buckling load is more significant than Winkler parameter. With the increase in the shear modulus, the fundamental frequency and critical buckling load increases.

7. With the increase in temperature and moisture concentration, the fundamental frequency and critical buckling load decrease.

8. The value of fundamental frequency and critical buckling load under full clamp boundary condition is higher than other boundary conditions however the effect of aforesaid parameters on fundamental frequency and critical buckling load are more sensible under full simply supported boundary condition than other boundary conditions.

9. Reddy's plate theory and hyperbolic shear deformation plate theory provide accurate and approximately same results for the hygro-thermal vibrational and buckling behavior of FG nanoplate.

References

- Ahn, S.J. (2004), *Least Squares Orthogonal Distance Fitting of Curves and Surfaces in Space*, Springer Science and Business Media, Berlin, Germany.
- Ahouel, M., Houari, M.A., Bedia, E.A. and Tounsi, A. (2016), "Size-dependent mechanical behavior of functionally graded trigonometric shear deformable nanobeams including neutral surface position concept", *Steel Compos. Struct.*, **20**(5), 963-981.
- Akgöz, B. and Civalek, Ö. (2011), "Buckling analysis of cantilever carbon nanotubes using the strain gradient elasticity and modified couple stress theories", *J. Comput. Theor. Nanosci.*, **8**(9), 1821-1827.
- Akgöz, B. and Civalek, Ö. (2016), "Bending analysis of embedded carbon nanotubes resting on an elastic foundation using strain gradient theory", *Acta Astronautica*, **119**, 1-12.
- Aluminum Association (1984), *Aluminum: Properties and Physical Metallurgy*, ASM International, Almere, Netherlands.
- Ansari, R. and Gholami, R. (2016), "Size-dependent modeling of the free vibration characteristics of postbuckled third-order shear deformable rectangular nanoplates based on the surface stress elasticity theory", *Compos. Part B: Eng.*, **95**, 301-316.
- Ansari, R. and Gholami, R. (2017), "Size-dependent buckling and postbuckling analyses of first-order shear deformable magneto-electro-thermo elastic nanoplates based on the nonlocal elasticity theory", *J. Struct. Stabil. Dynam.*, **17**(1), 1750014.
- Ansari, R., Ashrafi, M.A., Pourashraf, S. and Sahmani, S. (2015), "Vibration and buckling characteristics of functionally graded nanoplates subjected to thermal loading based on surface elasticity theory", *Acta Astronautica*, **109**, 42-51.
- Ansari, R., Faghish Shojaei, M., Mohammadi, V., Gholami, R. and Darabi, M.A. (2014), "Nonlinear vibrations of functionally graded Mindlin microplates based on the modified couple stress theory", *Compos. Struct.*, **114**, 124-134.
- Ansari, R., Faghish Shojaei, M., Mohammadi, V., Gholami, R. and Darabi, M.A. (2015), "A nonlinear shear deformable nanoplate model including surface effects for large amplitude vibrations of rectangular nanoplates with various boundary conditions", *J. Appl. Mech.*, **7**(5), 1550076.
- Attia, A., Bousahla, A.A., Tounsi, A., Mahmoud, S.R. and Alwabi, A.S. (2018), "A refined four variable plate theory for thermoelastic analysis of FGM plates resting on variable elastic foundations", *Struct. Eng. Mech.*, **65**(4), 453-464.
- Barati, M. R. and Shahverdi, H. (2016), "A four-variable plate theory for thermal vibration of embedded FG nanoplates under non-uniform temperature distributions with different boundary conditions", *Struct. Eng. Mech.*, **60**(4), 707-727.
- Barati, M.R. and Shahverdi, H. (2017), "An analytical solution for thermal vibration of compositionally

- graded nanoplates with arbitrary boundary conditions based on physical neutral surface position”, *Mech. Adv. Mater. Struct.*, **24**(10), 840-853.
- Barati, M.R., Zenkour, A.M. and Shahverdi, H. (2016), “Thermo-mechanical buckling analysis of embedded nanosize FG plates in thermal environments via an inverse cotangential theory”, *Compos. Struct.*, **141**, 203-212.
- Belabed, Z., Bousahla, A.A., Houari, M.A., Tounsi, A. and Mahmoud, S.R. (2018), “A new 3-unknown hyperbolic shear deformation theory for vibration of functionally graded sandwich plate”, *Earthq. Struct.*, **14**(2), 103-115.
- Beldjelili, Y., Tounsi, A. and Mahmoud, S.R. (2016), “Hygro-thermo-mechanical bending of S-FGM plates resting on variable elastic foundations using a four-variable trigonometric plate theory”, *Smart Struct. Syst.*, **18**(4), 755-786.
- Bellifa, H., Benrahou, K.H. and Bousahala, A.A. (2017), “A nonlocal zeroth-order shear deformation theory for nonlinear postbuckling of nanobeams”, *Struct. Eng. Mech.*, **62**(6), 695-702.
- Besseghei, A., Houari, M.A., Tounsi, A. and Mahmoud, S.R. (2017), “Free vibration analysis of embedded nanosize FG plates using a new nonlocal trigonometric shear deformation theory”, *Smart Struct. Syst.*, **19**(6), 601-614.
- Bloom, F. and Coffin, D.W. (2000), “Modelling the hygroscopic buckling of layered paper sheets”, *Math. Comput. Modelling*, **31**(8-9), 43-60.
- Bouafia, K., Kaci, A., Houari, M.A., Benzair, A. and Tounsi, A. (2017), “A nonlocal quasi-3D theory for bending and free flexural vibration behaviors of functionally graded nanobeams”, *Smart Struct. Syst.*, **19**(2), 115-126.
- Bouderba, B., Houari, M.A. and Tounsi, A. (2013), “Thermomechanical bending response of FGM thick plates resting on Winkler-Pasternak elastic foundations”, *Steel Compos. Struct.*, **14**(1), 85-104.
- Bouderba, B., Houari, M.A., Tounsi, A. and Mahmoud, S.R. (2016), “Thermal stability of functionally graded sandwich plates using a simple shear deformation theory”, *Struct. Eng. Mech.*, **58**(3), 397-422.
- Bounouara, F., Benrahou, K.H., Belkorissat, I. and Tounsi, A. (2016), “A nonlocal zeroth-order shear deformation theory for free vibration of functionally graded nanoscale plates resting on elastic foundation”, *Steel Compos. Struct.*, **20**(2), 227-249.
- Bousahla, A.A., Benyoucef, S., Tounsi, A. and Mahmoud, S.R. (2016), “On thermal stability of plates with functionally graded coefficient of thermal expansion”, *Struct. Eng. Mech.*, **60**(2), 313-335.
- Chaht, F.L., Kaci, A., Houari, M.A., Tounsi, A., Beg, O.A and Mahmoud, S.R. (2015), “Bending and buckling analyses of functionally graded material (FGM) size-dependent nanoscale beams including the thickness stretching effect”, *Steel Compos. Struct.*, **18**(2), 425-442.
- Chen, W.J. and Li, X.P. (2013), “Size-dependent free vibration analysis of composite laminated Timoshenko beam based on new modified couple stress theory”, *Archive Appl. Mech.*, **83**(3), 431-444.
- Civalek, Ö. (2013), “Nonlinear dynamic response of laminated plates resting on nonlinear elastic foundations by the discrete singular convolution-differential quadrature coupled approaches”, *Compos. Part B Eng.*, **50**, 171-179.
- Civalek, Ö. and Demir, C. (2016), “A simple mathematical model of microtubules surrounded by an elastic matrix by nonlocal finite element method”, *Appl. Math. Comput.*, **289**, 335-352.
- Daneshmehr, A., Rauabpoor, A. and Hadi, A. (2015), “Size dependent free vibration analysis of nanoplates made of functionally graded materials based on nonlocal elasticity theory with high order theories”, *J. Eng. Sci.*, **95**, 23-35.
- Duffy, D.G. (2015), *Green's Functions with Applications*. CRC Press, Florida, U.S.A.
- Ebrahimi, F. and Barati, M.R. (2016a), “Size-dependent thermal stability analysis of graded piezomagnetic nanoplates on elastic medium subjected to various thermal environments”, *Appl. Phys. A*, **122**(10), 910.
- Ebrahimi, F. and Barati, M.R. (2016b), “Temperature distribution effects on buckling behavior of smart heterogeneous nanosize plates based on nonlocal four-variable refined plate theory”, *J. Smart Nano Mater.*, **7**(3), 119-143.
- Ebrahimi, F. and Barati, M.R. (2016c), “Static stability analysis of smart magneto-electro-elastic heterogeneous nanoplates embedded in an elastic medium based on a four-variable refined plate theory”,

- Smart Mater. Struct.*, **25**(10), 105014.
- Ebrahimi, F. and Barati, M.R. (2016d), "Magneto-electro-elastic buckling analysis of nonlocal curved nanobeams", *Eur. Phys. J. Plus*, **131**(9), 346.
- Ebrahimi, F. and Barati, M.R. (2017a), "Damping vibration analysis of smart piezoelectric polymeric nanoplates on viscoelastic substrate based on nonlocal strain gradient theory", *Smart Mater. Struct.*, **26**(6), 065018.
- Ebrahimi, F. and Barati, M.R. (2017b), "Investigating physical field effects on the size-dependent dynamic behavior of inhomogeneous nanoscale plates", *Eur. Phys. J. Plus*, **132**(2), 88.
- Ebrahimi, F. and Barati, M.R. (2017c), "Buckling analysis of piezoelectrically actuated smart nanoscale plates subjected to magnetic field", *J. Intelligent Mater. Syst. Structures*, **28**(11), 1472-1490.
- Ebrahimi, F. and Barati, M.R. (2017d), "Magnetic field effects on dynamic behavior of inhomogeneous thermo-piezo-electrically actuated nanoplates", *J. Brazilian Soc. Mech. Sci. Eng.* **39**(6), 2203-2223.
- Ebrahimi, F. and Barati, M.R. (2018a), "Damping vibration analysis of graphene sheets on viscoelastic medium incorporating hygro-thermal effects employing nonlocal strain gradient theory", *Compos. Struct.*, **185**, 241-253.
- Ebrahimi, F. and Barati, M.R. (2018b), "Vibration analysis of size-dependent flexoelectric nanoplates incorporating surface and thermal effects", *Mech. Adv. Mater. Struct.*, **25**(7), 611-621.
- Ebrahimi, F. and Hosseini, S. (2016a), "Thermal effects on nonlinear vibration behavior of viscoelastic nanosize plates", *J. Therm. Stresses*, **39**(5), 606-625.
- Ebrahimi, F. and Hosseini, S. (2016b), "Double nanoplate-based NEMS under hydrostatic and electrostatic actuations", *Eur. Phys. J. Plus*, **131**(5), 160.
- Ebrahimi, F. and Salari, E. (2015), "Thermal buckling and free vibration analysis of size dependent Timoshenko FG nanobeams in thermal environments", *Compos. Struct.*, **128**, 363-380.
- Ebrahimi, F. and Shafiei, N. (2017), "Influence of initial shear stress on the vibration behavior of single-layered graphene sheets embedded in an elastic medium based on Reddy's higher-order shear deformation plate theory", *Adv. Mater. Struct.*, **24**(9), 761-772.
- Ebrahimi, F., Hamed, S. and Hosseini, S. (2016), "Nonlinear electroelastic vibration analysis of NEMS consisting of double-viscoelastic nanoplates", *Appl. Phys. A*, **122**(10), 922.
- El-Haina, F., Bousahla, A.A., Tounsi, A. and Mahmoud, S.R. (2017), "A simple analytical approach for thermal buckling of thick functionally graded sandwich plates", *Struct. Eng. Mech.*, **63**(5), 585-595.
- Eringen, A.C. (1972), "On nonlocal elasticity", *J. Eng. Sci.*, **10**(3), 233-248.
- Eringen, A.C. (1983), "On differential equations of nonlocal elasticity and solutions of screw dislocation and surface waves", *J. Appl. Phys.*, **54**(9), 4703-4710.
- Foroushani, S.S. and Azhari, M. (2016), "Nonlocal buckling and vibration analysis of thick rectangular nanoplates using finite strip method based on refined plate theory", *Acta Mechanica*, **227**(3), 721-742.
- Gholami, R., Ansari, R. and Gholami, Y. (2017), "Size-dependent bending, buckling and vibration of higher-order shear deformable magneto-electro-thermo-elastic rectangular nanoplates", *4*(6), 065702.
- Gürses, M., Civalek, Ö., Korkmaz, A.K. and Ersoy, H. (2009), "Free vibration analysis of symmetric laminated skew plates by discrete singular convolution technique based on first-order shear deformation theory", *J. Numer. Methods Eng.*, **79**(3), 290-313.
- Gurtin, M.E. and Murdoch, A.I. (1975), "A continuum theory of elastic material surfaces", *Arch. Rational Mech. Anal.*, **57**(4), 291-323.
- Gurtin, M.E. and Murdoch, A.I. (1978), "Surface stress in solids", *J. Solids Struct.*, **14**(6), 431-440.
- Habibi, N., Ahmadi, O. and Ahmadi, S.R. (2016), "Vibration of nanoplate on elastic foundation in thermal environment", *International Conference on Nanotechnology*, Istanbul, Turkey, August.
- Hachemi, H., Kaci, A., Houari, M.A., Bourada, M., Tounsi, A. and Mahmoud, S.R. (2017), "A new simple three-unknown shear deformation theory for bending analysis of FG plates resting on elastic foundations", *Steel Composite Structures*, **25**(6), 717-726.
- Hamidi, A., Houari, M. A., Mahmoud, S. R., & Tounsi, A. (2015), "A sinusoidal plate theory with 5-unknowns and stretching effect for thermomechanical bending of functionally graded sandwich plates", *Steel Compos. Struct.*, **18**(1), 235-253.

- Hosseini, M., Jamalpoor, A. and Fath, A. (2017), "Surface effect on the biaxial buckling and free vibration of FGM nanoplate embedded in visco-Pasternak standard linear solid-type of foundation", *Meccanica*, **52**(6), 1381-1396.
- Houari, M.A., Tounsi, A., Bessaim, A. and Mahmoud, S.R. (2016), "A new simple three-unknown sinusoidal shear deformation theory for functionally graded plates", *Steel Compos. Struct.*, **22**(2), 257-276.
- Hull, R. (1999), *Properties of Crystalline Silicon*. IET, London, United Kingdom.
- Ibach, H. (1997), "The role of surface stress in reconstruction, epitaxial growth and stabilization of mesoscopic structures", *Surface Sci. Rep.*, **29**(5-6), 195-263.
- Javaheri, R. and Eslami, M.R. (2002), "Thermal buckling of functionally graded plates", *AIAA journal*, **40**(1), 162-169.
- Jones, R.M. (2006), *Buckling of Bars, Plates and Shells*, Bull Ridge Publishing, Virginia, U.S.A.
- Jung, W.Y., Park, W.T. and Han, S.C. (2014), "Bending and vibration analysis of S-FGM microplates embedded in Pasternak elastic medium using the modified couple stress theory", *J. Mech. Sci.*, **87**, 150-162.
- Karami, B., Janghorban, M. and Tounsi, A. (2018a), "Nonlocal strain gradient 3D elasticity theory for anisotropic spherical nanoparticles", *Steel Compos. Struct.*, **27**(2), 201-216.
- Karami, B., Janghorban, M. and Tounsi, A. (2018b), "Variational approach for wave dispersion in anisotropic doubly-curved nanoshells based on a new nonlocal strain gradient higher order shell theory", *Thin-Wall. Struct.*, **129**, 251-264.
- Karimi, M. and Shahidi, A.R. (2015), "Finite difference method for sixth-order derivatives of differential equations in buckling of nanoplates due to coupled surface energy and non-local elasticity theories", *J. Nano Dimension*, **6**(5), 525-538.
- Karimi, M., Haddad, H.A. and Shahidi, A.R. (2015), "Combining surface effects and non-local two variable refined plate theories on the shear/biaxial buckling and vibration of silver nanoplates", *Micro Nano Lett.*, **10**(6), 276-281.
- Khetir, H., Bouadjra, M.B., Houari, M.A., Tounsi, A. and Mahmoud, S.R. (2017), "A new nonlocal trigonometric shear deformation theory for thermal buckling analysis of embedded nanosize FG plates", *Struct. Eng. Mech.*, **64**(4), 391-402.
- Link International (2016), What are coefficients of expansion and why are they important?;, Link International, Muizenberg, South Africa. www.linkinternationalkl.com/what-are-coefficients-of-expansion-and-why-are-they-important/.
- Lu, C.F., Lim, C.W. and Chen, W.Q. (2009), "Size-dependent elastic behavior of FGM ultra-thin films based on generalized refined theory", *J. Solids Struct.*, **46**(5), 1176-1185.
- Malekzadeh, P. (2007), "A differential quadrature nonlinear free vibration analysis of laminated composite skew thin plates", *Thin-Wall. Struct.*, **45**(2), 237-250.
- Marie, J.M. (2012), *Composite Materials: Mechanical Behavior and Structural Analysis*, Springer Science and Business Media, Berlin. Germany.
- Menasria, A., Bouhadra, A., Tounsi, A., Bousahla, A.A. and Mahmoud, S.R. (2017), "A new and simple HSDT for thermal stability analysis of FG sandwich plates", *Steel Compos. Struct.*, **25**(2), 157-175.
- Mercan, K. and Civalek, Ö. (2016), "DSC method for buckling analysis of boron nitride nanotube (BNNT) surrounded by an elastic matrix", *Compos. Struct.*, **143**, 300-309.
- Mokhtar, Y., Heireche, H., Bousahla, A.A., Houari, M.A., Tounsi, A. and Mahmoud, S.R. (2018), "A novel shear deformation theory for buckling analysis of single layer graphene sheet based on nonlocal elasticity theory", *Smart Struct. Syst.*, **21**(4), 397-405.
- Mondolfo, L.F. (2013), *Aluminum Alloys: Structure and Properties*, Elsevier, Amsterdam, Netherlands.
- Mouffoki, A., Bedia, E.A., Houari, M.A., Tounsi, A. and Mahmoud, S.R. (2017), "Vibration analysis of nonlocal advanced nanobeams in hygro-thermal environment using a new two-unknown trigonometric shear deformation beam theory", *Smart Struct. Syst.*, **20**(3), 369-383.
- Nguyen, N.T., Hui, D., Lee, J. and Xuan, H.N. (2015), "An efficient computational approach for size-dependent analysis of functionally graded nanoplates", *Comput. Methods Appl. Mech. Eng.*, **297**, 191-218.
- Panyatong, M., Chinnaboon, B. and Chucheepsakul, S. (2016), "Free vibration analysis of FG nanoplates

- embedded in elastic medium based on second-order shear deformation plate theory and nonlocal elasticity”, *Compos. Struct.*, **153**, 428-441.
- Praveen, G.N. and Reddy, J.N. (1998), “Nonlinear transient thermoelastic analysis of functionally graded ceramic-metal plates”, *J. Solids Struct.*, **35**(33), 4457-4476.
- Qian, L.F., Batra, R.C. and Chen, L.M. (2004), “Static and dynamic deformations of thick functionally graded elastic plates by using higher-order shear and normal deformable plate theory and meshless local Petrov-Galerkin method”, *Compos. Part B: Eng.*, **35**(6), 685-697.
- Reddy, B.S., Kumar, J.S., Reddy, C.E. and Reddy, K.V. (2013), “Buckling analysis of functionally graded material plates using higher order shear deformation theory”, *J. Compos.*, **2013**, 808764.
- Reddy, J.N. (2006), *Theory and Analysis of Elastic Plates and Shells*, CRC press, Florida, U.S.A.
- Reddy, J.N. (2010), “Nonlocal nonlinear formulations for bending of classical and shear deformation theories of beams and plates”, *J. Eng. Sci.*, **48**(11), 1507-1518.
- Reddy, J.N. (2011), “A general nonlinear third-order theory of functionally graded plates”, *J. Aerosp. Lightweight Struct.*, **1**(1), 1-21.
- Shaat, M., Mahmoud, F.F., Alshorbagy, A.E. and Alieldin, S.S. (2013), “Bending analysis of ultra-thin functionally graded Mindlin plates incorporating surface energy effects”, *J. Mech. Sci.*, **75**, 223-232.
- Shahram, P., Ganti, S., Ardebili, H. and Alizadeh, A. (2004), “On the scaling of thermal stresses in passivated nanointerconnects”, *J. Appl. Phys.*, **95**(5), 2763-2769.
- Shen, H.S. (2016), *Functionally Graded Materials: Nonlinear Analysis of Plates and Shells*, CRC press, Florida, U.S.A.
- Shen, J., Wang, H. and Zheng, S. (2018), “Size-dependent pull-in analysis of a composite laminated micro-beam actuated by electrostatic and piezoelectric forces: Generalized differential quadrature method”, *J. Mech. Sci.*, **135**, 353-361.
- Shu, C. (2012), *Differential Quadrature and Its Application in Engineering*, Springer Science and Business Media, Berlin, Germany.
- Sobhy, M. (2015), “A comprehensive study on FGM nanoplates embedded in an elastic medium”, *Compos. Struct.*, **134**, 966-980.
- Swarnakar, A.K., Biest, O.V. and Vanhellemont, J. (2014), “Determination of the Si Young’s modulus between room and melt temperature using the impulse excitation technique”, *Physica Status Solidi*, **11**(1), 150-155.
- Vasiliev, V.V. and Morozov, E.V. (2013), *Advanced Mechanics of Composite Materials and Structural Elements*. Newnes Books, Oxford, United Kingdom.
- Yazid, M., Heireche, H., Tounsi, A., Bousahla, A.A. and Houari, M.A. (2018), “A novel nonlocal refined plate theory for stability response of orthotropic single-layer graphene sheet resting on elastic medium”, *Smart Struct. Syst.*, **21**(1), 15-25.
- Youcef, D.O., Kaci, A., Benzair, A., Bousahla, A.A. and Tounsi, A. (2018), “Dynamic analysis of nanoscale beams including surface stress effects”, *Smart Struct. Syst.*, **21**(1), 65-74.
- Zare, M., Nazemnezhad, R. and Hashemi, S.H. (2015), “Natural frequency analysis of functionally graded rectangular nanoplates with different boundary conditions via an analytical method”, *Meccanica*, **50**(9), 2391-2408.
- Zhang, D.G. and Zhou, Y.H. (2008), “A theoretical analysis of FGM thin plates based on physical neutral surface”, *Comput. Mater. Sci.*, **44**(2), 716-720.
- Zidi, M., Tounsi, A., Houari, M.A. and Bég, O.A. (2014), “Bending analysis of FGM plates under hydro-thermo-mechanical loading using a four variable refined plate theory”, *Aerosp. Sci. Technol.*, **34**, 24-34.